ISSN 1813-2065

IRAQI JOURNAL OF APPLIED PHYSICS

VOLUME 2 ISSUES 1&2 2006

Sponsored and Published by

THE IRAQI SOCIETY FOR ALTERNATIVE AND RENEWABLE ENERGY SOURCES AND TECHNIQUES (I.S.A.R.E.S.T.)

SPONSORED AND PUBLISHED BY

THE IRAQI SOCIETY FOR ALTERNATIVE AND RENEWABLE ENERGY SOURCES AND TECHNIQUES (I.S.A.R.E.S.T.)

EDITORIAL BOARD

Dayah N. RAOUF
Editor-In-Chief
School of Applied Sciences
University of Technology,
IRAQ
dnraouf2005@yahoo.com

Walid K. HAMOUDI
Member
School of Applied Sciences
University of Technology
IRAQ
walid_khk@hotmail.com

Raid A. ISMAIL
Member
Physics Science and Research Center,
Ministry of Science and Technology,
IRAQ
raidismail@yahoo.com

Raad A. KHAMIS
Member
School of Applied Sciences
University of Technology
IRAQ
drraad2001@yahoo.com

Oday A. HAMADI
Managing Editor
P. O. Box 55159,
Baghdad 12001,
IRAQ
odayata2001@yahoo.com

ADVISORY BOARD

Chang Hee NAM
Professor
Coherent X-Ray Research Center,
Korean Advanced Institute of Science
and Technology, Teajon,
KOREA

Marc BURGELMAN
Professor
Electronics and Information
Systems (ELIS),
University of Gent, Gent
BELGIUM

Andrei KASIMOV
Professor
Solar Energy Conversion Group,
Institute of Material Science,
National Academy of Science,
UKRAINE

Xueming LIU
Professor
Department of Electronic
Engineering, Tsinghua University,
Beijing, CHINA

Ashok KUMAR
Professor
Harcourt Butler Technological
Institute, Kanpur - 208 002,
INDIA

Yanko SAROV
Assistant Professor
Central Lab. of Optics
Bulgarian Academy of Science
Sofia, BULGARIA

Mansoor SHEIK-BAHAE
Associate Professor
Department of Physics and
Astronomy, University of New
Mexico, Albuquerque, U.S.A

Intisar F. RAMLEY
Professor
MERIDEX Software
Corporation, Richmond,
CANADA

Franko KUEPPERS
Assistant Professor
College of Optical Sciences,
University of Arizona, Tucson,
U.S.A

Mohammed A. HABEEB
Professor
Physics Sciences and Research
Center, Ministry of Science and
Technology, Baghdad, IRAQ

Mazin M. ELIAS
Professor
Laser Institute for Postgraduates
University of Baghdad
Baghdad, IRAQ

El-Sayed M. FARAG
Professor
Department of Basic Sciences
College of Engineering
Al-Minofiya University, EGYPT

Abdullah M. SUHAIL
Assistant Professor
Department of Physics
College of Science
University of Baghdad, IRAQ

Manal J. AL-KINDY
Assistant Professor
Department of Electronic and
Communications Engineering
Al-Nahrain University, IRAQ

Mutaz S. ABDUL-WAHAB
Assistant Professor
Electric and Electronic
Engineering, University of
Technology, Baghdad, IRAQ

Kais A. AL-NAIEEMY
Assistant Professor
Department of Physics
College of Science
University of Baghdad, IRAQ

Muhammad A. HUSSAIN
Assistant Professor
Department of Laser and
Optoelectronics Engineering
Al-Nahrain University, IRAQ

Khaled A. AHMED
Assistant Professor
Department of Physics
College of Science
Al-Mustansiriya University, IRAQ

ISSN 1813-2065

Organized by I.S.A.R.E.S.T.

INVITATION TO ATTEND

To introduce more about the alternative and renewable energy sources and techniques, I.S.A.R.E.S.T. invites you to attend the scientific lectures organized by I.S.A.R.E.S.T. You are requested to contact the secretary of the society and register your attendance. The lectures can be held earlier due to the registered requests.

INVITATION TO PARTICIPATE

To all they would like to submit seminars or scientific lectures during the third semester of the **I.S.A.R.E.S.T.** (July, August and September) in 2006, you are kindly requested to contact the secretary of the **I.S.A.R.E.S.T.** for date and presentation arrangements of the seminars or lectures. Please, do not hesitate to participate in our activities, this chance might be required by young scientists in our country, IRAQ, to develop and grow as well as introduce the professors and experts in field. You could find us on the post address, emails and mobile below:

Postal:

P. O. Box 55259, Baghdad 12001, IRAQ

Emails:

irq_appl_phys@yahoo.com
editor_ijap@yahoo.com
odayata2001@yahoo.com

ISAREST

Mobile:

00964-7901274190

Junction Characteristics of Wide-Emitter (p)CdS-(n)Si-(p)Si Heterojunction Transistor

Raid A.W. Ismail [1*]
Jenan T. Jabar [1]
Omar A.S. Abdulrazaq [2]

[1] *School of Applied Sciences, University of Technology, Baghdad, IRAQ*
** raidismail@yahoo.com*
[2] *NASSR State Company, Ministry of Industry and Minerals, Baghdad, IRAQ*

Fabrication and characterization of feasible heterojunction bipolar transistor (HBT) made by depositing of p-type CdS film on monocrystalline silicon homojunction were demonstrated. The ideality factors (n) of emitter-base and base-collector abrupt junctions were 1.6 and 1.8 respectively. The transistor exhibited current gain β_{dc} as high as 360.

Keywords: *TFT, Heterojunction, Silicon devices*

Received: 18 December 2005, Revised: 1 February 2006, Accepted: 18 February 2006

1. Introduction

Possibility of using wide-bandgap emitter injection efficiency of a transistor was first proposed by Schockley [1] and later analyzed by Kroemer [2] in 1957. Even though this idea promised large advantages over the existing transistors, very little attention was paid towards the realization of such a transistor due to rapid advances in the technology of homo-transistor [3, 4]. With the advancement in the "state of art" of heterojunction fabrication [5-7], the interest in the heterojunction bipolar transistors (HBTs) has been lately revived [8-11]. The recent trend in high-speed silicon technologies has produced remarkable advances in silicon-based HBT. The physical structure of such a transistor is composed of a hetero-layer (emitter) grows on a p-n Si diode. The grown layer can be formed by several techniques. Among the various techniques, spray pyrolysis was used successfully in producing heterojunction [12,13]. In this paper, a newly found junction characteristics of the (p)CdS-(n)Si-(p)Si HBT are presented where p-CdS was grown by spray pyrolysis.

2. Experiment

Boron-doped single crystal p-Si wafer with sheet resistivity of about 35.6 Ω/sq. and orientation of (100) has been thermally diffused by phosphorus using thermal diffusion system. The diffused layer was heavily doped (2.1×10^{18}cm^{-3}) and the junction was made to be 0.5μm. Wide-emitter p-CdS:Ag layer with thickness of 1μm and area of 0.7mm^2 has been deposited onto n-Si side by pyrolytic spraying of an aqueous solution of 0.2M $CdCl_2$, 0.18M thiourea and 0.006M $AgNO_3$ with a deposition rate of about 2nm/s. The preparation substrate temperature was 350°C. Figure 1 depicts a photograph of spray pyrolysis apparatus used in this study. Indium, gold and aluminium electrodes were deposited by thermal evaporation through special masks on CdS:Ag, n-Si and p-Si respectively. Figure (2) displays energy band diagram of fabricated HBT. Hall measurements were done to estimate the conductivity type of CdS:Ag layer deposited on glass substrate. C-V measurement of HBT at 1MHz was carried out using LCZ system.

Fig. (1): Spray pyrolysis system used to grow CdS:Ag layer

3. Results and Discussion

Pure CdS is normally an n-type semiconductor. This type of conductivity is essentially due to the non-stoichiometry arisen from the excess Cd in the CdS lattice (enriched-Cd). So that it is previously used as a heterojunction transistor type n-p-n with n-pSi diode [14] and/or window layer for UV-enhancement in double junctions with p-nSi photodiodes [15]. Producing p-type CdS can be obtained by silver doping of CdS. In this doping, Cd^{+2} will be replaced by Ag^{+} in the lattice of CdS microcrystallites. This replacement will result in less sulfur deficiency because the anion (S^{-2}) has a valence number greater than the cation (Ag^{+}) and enriched-S CdS will be produced. This type of defects leads to abundant of holes and p-type CdS will be formed. Hall measurement of Ag-doped CdS shown in Figure 3. This figure shows a p-type behavior, so that it will form a heterojunction transistor type p-n-p with p-nSi.

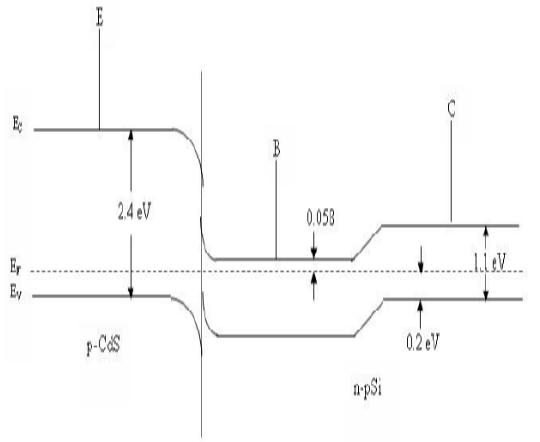

Fig. (2): An equilibrium band diagram of (p)CdS-(n)Si-(p)Si HBT

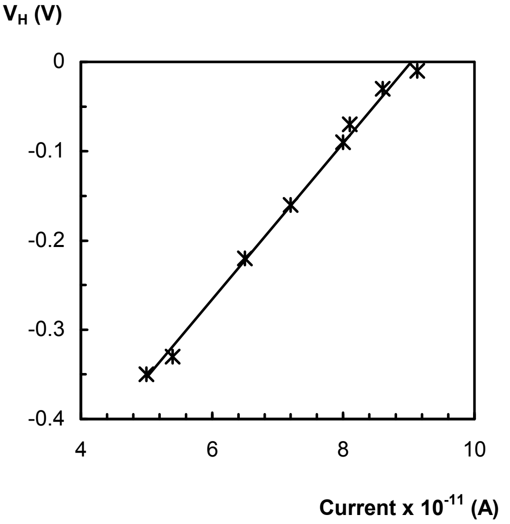

Fig. (3): The relationship between Hall voltage and passing current for p-CdS film

The two junctions of the triode have been characterized separately using I-V measurements. Figure 4a demonstrates I_E-V_{EB} characteristics (floating collector) where V_{BE} and I_E respectively represent the applied voltage across emitter-base junction and the flow current due to this voltage. The forward current of this junction is distinguished by two regions, the first (less than 0.3V bias voltage) region represents recombination mechanism while the second (greater than 0.3V bias voltage) indicates tunneling mechanism. The transport mechanism then shows good conformity with the tunneling-recombination model. This result is in full agreement with those of p-CdS/n-Si heterodiode [16]. Figure 4b illustrates the I_C-V_{BC} characteristics (floating emitter) where V_{BC} and I_C respectively represent the applied voltage across base-collector junction and the flowing current due to this voltage. The I_C-V_{BC} curve of this junction shows a behavior in coincidence with that of Shockley model **($I=I_0 \exp(qV/nkT)$)**. High leakage current reflects the heavily doped layer. From the two plots of Figure 4, the ideality factor (n) of emitter-base and base-collector junctions were as low as 1.6 and 1.8, respectively, indicating high quality of both junctions. Figure 5 presents C_{EB}-V_{EB} and C_{BC}-V_{BC} curves where the subscripts refer to the emitter-base and base-collector, respectively. It is shown from the figure that the emitter-base junction capacitance is smaller than that of base-collector. This can be elucidated by the low carrier concentration of the wide-emitter. On the other hand, these two junctions are abrupt types.

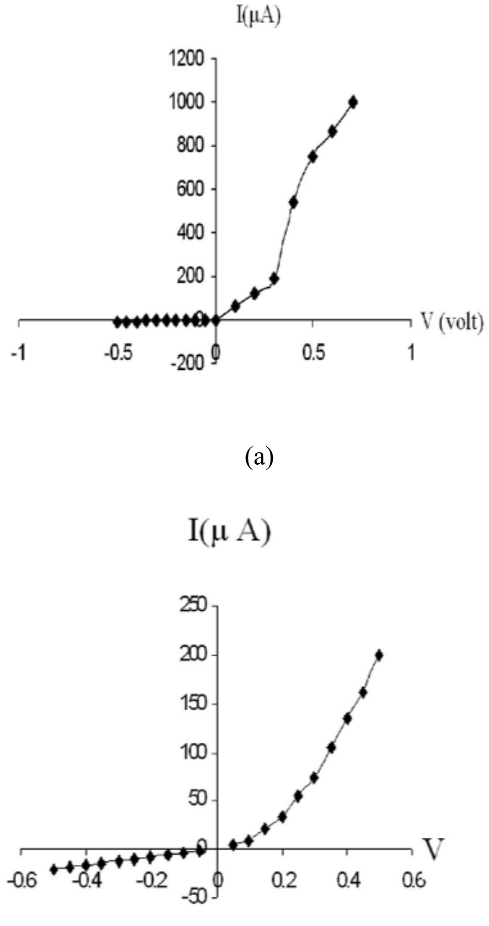

(a)

(b)

Fig. (4)**: I-V characteristics for (a): (p)CdS-(n)Si junction and (b): (n)Si-(p)Si junction**

The dc beta (β_{dc}) of the common-emitter HBT has been directly measured and gave a value of 360, this high value has been obtained using material for which there is a large lattice mismatch of roughly 8% and indicates that interfacial recombination is much less than has been generally anticipated, this is mainly due to forming the gate layer (the base) with its high electron density in defect-free single-crystal material. The experimental HBT constructed in the present work is not optimized in any way, but serves merely to demonstrate the feasibility of transistor action. Considerable further research remains to be done to optimize the transistor performance and to ascertain the best design parameters.

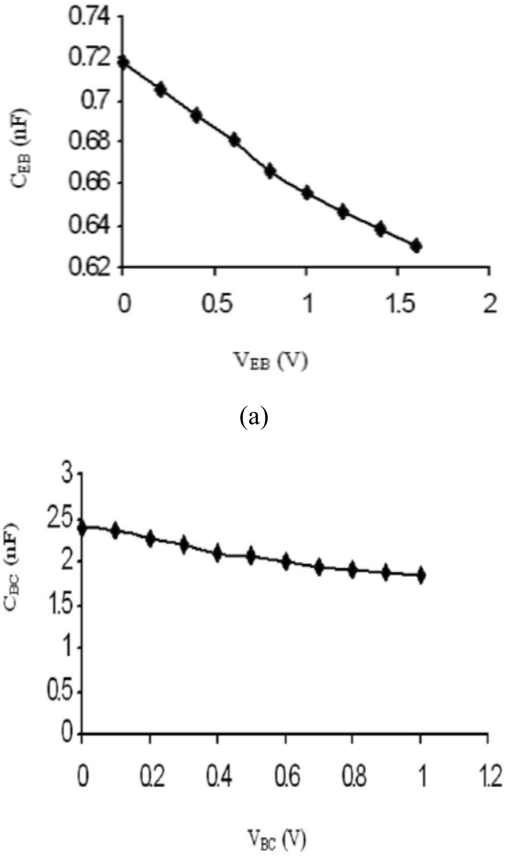

(a)

(b)

Fig. (5): C-V characteristics of the (p)CdS-(n)Si-(p)Si HBT junctions

4. Conclusions

A high dc performance heterojunction bipolar transistor has been realized by the low-cost spray pyrolysis technique. This technique allows good price/quality ratio. The relatively high value of dc beta (360) demonstrates clearly that the HBT type (p)CdS-(n)Si-(p)Si is a practical proposition.

References

[1] W. Shockley, U.S. Patent No. 2, 569, 347 (September 25, 1951).
[2] H. Kroemer, *Proc. IRE*, 45, 1535 (1989).
[3] D.J. Roulston, **"Bipolar Semiconductor Devices"**, McGraw Hill, New York, 1990.
[4] K.K. Ng, **"Complete Guide to Semiconductor Devices"**, McGraw Hill, New York, 1995, 240.
[5] Hermanm, *Solar Mater. Solar Cells*, 66, 85 (1998).
[6] J. Kolodzey, *Vacuum Solutions*, 9, 5 (1999).
[7] D. Song, J. Zhao, A. Wang, P. Widenborg, W. Chin and A.G. Aberly, 17th European PV Conference, Munich, 2001, p. 1.
[8] F. Chin and P. Bhattacharya, *IEEE Trans. Electron Devices*, 36, 2183 (1989).
[9] P.R. Berger, N. Chand and N.K. Dutta, *Appl. Phys. Lett.*, 59, 1099 (1991).
[10] R.W. Sandage and J.A. Connelly, in *IEDM Tech. Dig.*, 171 (1995).
[11] W. Zhang, M. Chan, S.K. Fung and P.K. Ko, *IEEE Electron Devices Lett.*, 19, 435 (1998).
[12] T. Ishida, H. Konno, H. Kobayashi and Y. Nakato, *J. Electrochem. Soc.*, 141, 1357 (1994).
[13] H. Kobayashi, S. Techibana, K. Yamanaka, Y. Nakato and K. Yoneda, *J. Appl. Phys.*, 81, 7630 (1997).
[14] S. Brojdo, T.J. Riley and G.T. Wright, Brit. *J. Appl. Phys.*, 16,133 (1965).
[15] P. Laou, "Heterojunction on Monocrystalline Silicon", Dissertation Abstracts, McGill University, Canada, 1994, MAI 33/04, p. 1307, August 1995.
[16] R.A. Ismail, A.E. Al-Samarai and O.A.A. Sultan, *J. Eng. Technol.* (printed in Iraq), 20, 486 (2001).

This article was reviewed at The Laboratory of Electronics and Chemical Physics, Luis Pasteur University, Strasburg, FRANCE and Department of Physics, Harcourt Butler Technological Institute, Kanpur, INDIA

CONFERENCES

UPCOMING IN 2006

7th National Symposium on Display Holography
10 - 14 July 2006 , St. Asaph, United Kingdom
SPIE Europe is a technical co-sponsor

5th World Congress of Biomechanics
29 July - 4 August 2006 , Munich, Germany
SPIE is a cooperating organization

SPIE Optics & Photonics
13 - 17 August 2006 , San Diego, California USA
co-located with SPIE's 51st Annual Meeting
Advance Registration Ends 28 July 2006
Exhibition

Micro- to Nano-Photonics: ROMOPTO 2006
28 - 31 August 2006 , Sibiu, Romania
Sponsored by SPIE Romania Chapter. SPIE will publish proceedings.

SPIE APOC 2006 Asia-Pacific Optical Communications
3 - 7 September 2006 , Gwangju, South Korea
Abstracts Due 31 March 2006

Optics in the Southeast 2006 & High Capacity Optical Networks and Enabling Technologies 2006
6 - 8 September 2006 , Charlotte, North Carolina USA
Abstracts Due 30 June 2006

Remote Sensing - An SPIE Europe Event
11 - 14 September 2006 , Stockholm, Sweden
co-located with the SPIE Europe Symposium on
Optics and Photonics for Security and Defense
Advance Registration Ends 24 August 2006

Optics/Photonics in Security and Defense
An SPIE Europe Event
11 - 14 September 2006 , Stockholm, Sweden
collocated with European Remote Sensing
Advance Registration Ends 24 August 2006

Speckle 2006 International Conference
13 - 15 September 2006 , Nimes, France
SPIE is a cooperating organization and is publishing proceedings

27th International Congress on High-Speed Photography and Photonics
17 - 22 September 2006 , Xi'an, China
SPIE is publishing the proceedings

6th Annual Mirror Technology Days in the Government
18 - 20 September 2006 , Kirtland AFB, Albuquerque, New Mexico USA
SPIE is a co-sponsor

Qusay K. Ahmed
Mahdi S. Al-Ali[*]

Ministry of Science and Technology, Applied Physics Research Center, Baghdad, IRAQ
** mahdealali2000@yahoo.com*

New Method for Calculating Cumulative Line Energy Using Pupil Function Technique

A new relation has been derived to calculate the cumulative line energy (CLE) by using the pupil function technique for an optical system of a circular aperture. The relation was solved by numerical integration namely Gauss method for optical system free of aberration and for different focus error values. The cumulative line energy of an optical system suffering secondary spherical aberration in its optimal condition was calculated.

Keywords: *Cumulative line energy, pupil function, circular aperture*

Received: 23 March 2005, Revised: 1 February 2006, Accepted: 8 June 2006

1. Introduction

The importance of line spread function does not differ from the point spread function where both of them serve the same purpose, which is the high quality of the optical system. Yet, the line object is an infinity of illuminating points, hence the intensity given by this object in its shape is better than that of the point object. It was found that a considerable amount of aberration can influence the image shape produced by a point object, which makes it difficult to determine the efficiency of the optical system due to the difficulty of defining the central intensity. A condition of this type can be avoided by using a line source.

Barakat and Houston [1] calculated the line spread function by using an incoherent line source operating with a circular aperture in a rotationally symmetrical aberration. They [2] also studied the effect of the asymmetric aberrations on the line object image having third order coma aberration of different azimuth angels. Tschunko [3] used annular aperture of different central obscuration rates to calculate the line spread function of optical system free from aberration. He also used rectangular aperture of different widths and lengths and of different central obscuration ratios as well.

Kirillovskii and Krynin [4] studied the image quality using TV modified method to specify the line spread function.

2. Cumulative Line Energy (CLE)

To know whether the designed optical system has a high degree of efficiency, the specifications of the produced image were accurately examined. The most important output of the optical systems is the calculation of energy on the image plane.

The energy formed on the image produced from using a line source is known as cumulative line energy (CLE). This function is more important than the intensity scale in the image of the line object since it depends on the value of energy curve descent which does not lose its characteristics no matter how much the value of aberration increases. Friedman [5] was able to calculate the CLE of a coherent source. More recently, Abdulrazak [6] used a slot of changeable width to study diffraction at the best image plane and other focal planes as well.

The cumulative line energy (CLE) is calculated depending on the pupil function by performing integration on the line spread function $L(z')$ within the required limits from $-z_o$ to z_o as shown in Fig. (1).

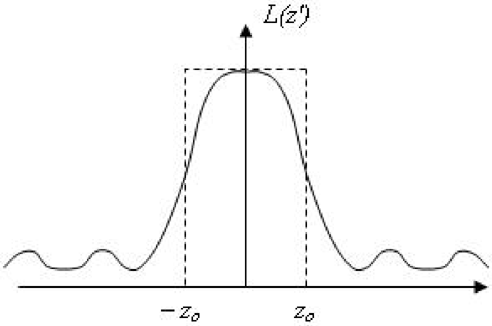

Fig. (1): Cumulative line energy (CLE) calculated from LSF

The distribution of intensity in the image of the incoherently illuminated line object is given by the following equation [7]:

$$LSF = \int_y \int_{x_1} \int_x f(x,y) \cdot f^*(x_1,y) \cdot e^{iz'x} \cdot e^{-iz'x_1} dx dx_1 dy \quad (1)$$

where z' is the image dimensionless coordinate, $f(x,y)$, $f^*(x1,y)$ are the exit pupil function and its complex conjugate, respectively, and x, x_1, y are the coordinates of both exit pupil function and its complex conjugate.

The exit pupil function is defined according to the circular aperture the center of which applies on the optical axis as follows:

$$x^2 + y^2 = 1 \qquad \text{and} \qquad x_1^{\,2} + y^2 = 1 \tag{2}$$

The cumulative line energy $Li(z_o)$ is defined by the following relation:

$$Li(z_0) = \int_{-z_0}^{z_0} L(z')dz' \tag{3}$$

Substituting equation (1) in equation (3), we obtain:

$$Li(z_0) = \int_y \int_{x_1} \int_x f(x,y) \cdot f^*(x_1,y)dxdx_1dy \cdot \int_{-z_0}^{z_0} e^{iz'(x-x_1)}dz' \tag{4}$$

Solving the last integration of equation (4), we get

$$Li(z_0) = N \int_y \int_{x_1} \int_x f(x,y) \cdot f^*(x_1,y) \cdot \frac{\sin[z_0(x-x_1)]}{(x-x_1)} dxdx_1dy \tag{5}$$

To find the normalizing factor (N), the cumulative line energy $Li(z_o)$ equals one when z_o approaches infinity. For simplicity, we consider the optimal condition that is aberration function $W(x,y)=0$ when $f(x,y) = f^*(x_1,y) = 1$

That is:

$$Li(z_0) = N \int_y \int_{x_1} \int_x \frac{\sin[z_0(x-x_1)]}{(x-x_1)} dxdx_1dy \tag{6}$$

Taking the limit of integration of the equation (6) when z_o approaches infinity, we obtain:

$$1 = \pi \cdot N \int_y \int_{x_1} \int_x \lim_{z_0 \to \infty} \frac{\sin[z_0(x-x_1)]}{\pi \cdot (x-x_1)} dxdx_1dy \tag{7}$$

A requirement of Dirac delta function [8] is:

$$\delta(x-x_1) = \lim_{z_o \to \infty} \frac{\sin[z_0(x-x_1)]}{\pi(x-x_1)} \tag{8}$$

Substituting equation (8) by equation (7) with reference to equation (2), it becomes possible to make integration in the following formula:

$$1 = \pi \cdot N \int_{-1}^{1} \int_{-\sqrt{1-y^2}}^{\sqrt{1-y^2}} \int_{-\sqrt{1-y^2}}^{\sqrt{1-y^2}} \delta(x-x_1)\, dxdx_1dy \tag{9}$$

There is one solution for the Dirac delta function and that is when $x=x_1$ so

$$\int_{-\sqrt{1-y^2}}^{\sqrt{1-y^2}} \delta(x-x_1)dx = 1 \tag{10}$$

The equation (9), therefore, becomes

$$1 = \pi \cdot N \int_{-1}^{1} \int_{-\sqrt{1-y^2}}^{\sqrt{1-y^2}} dxdy \tag{11}$$

By simplifying equation (11), we get the value of the normalizing factor (N) as follows:

$$N = \frac{1}{\pi^2} \qquad \text{For the circular aperture}$$

After the substitution of the normalizing factor value (N), equation (5) can be written as follows:

$$Li(z_0) = \frac{1}{\pi^2} \int_y \int_{x_1} \int_x f(x,y) \cdot f^*(x_1,y) \cdot \frac{\sin[z_0(x-x_1)]}{(x-x_1)} dxdx_1dy \tag{12}$$

As

$f(x,y) = e^{ikW(x,y)}$ and $f^*(x,y) = e^{-ikW(x,y)}$. Hence

$$Li(z_0) = \frac{1}{\pi^2} \int_{-1}^{1} \int_{-\sqrt{1-y^2}}^{\sqrt{1-y^2}} \int_{-\sqrt{1-y^2}}^{\sqrt{1-y^2}} e^{ik[W(x,y)-W(x_1,y)]} \cdot \frac{\sin[z_0(x-x_1)]}{(x-x_1)} dxdx_1dy \tag{13}$$

where $W(x,y)$ is the aberration function, $k=2\pi/\lambda$ is the wave number and λ is the wavelength.

As the cumulative line energy (CLE) is a real value, so the imaginary limit is equal to zero. Accordingly, equation (13) becomes

$$Li(z_0) = \frac{1}{\pi^2} \int_{-1}^{1} \int_{-\sqrt{1-y^2}}^{\sqrt{1-y^2}} \int_{-\sqrt{1-y^2}}^{\sqrt{1-y^2}} \cos[k\{W(x,y) - W(x_1,y)\}] \cdot \frac{\sin z_0(x-x_1)}{(x-x_1)} dxdx_1dy \tag{14}$$

The equation (14) represents the cumulative line energy of an optical system operating with circular aperture. It can be used for other apertures in the optical system by changing the limit of integration and the normalizing factor (N).

3. Results and Discussion

The equation (14) cannot be solved through ordinary integration methods. The solution, therefore, requires using one of the special numerical integration methods. Gauss method was used since it provides high accuracy in the calculation of integration.

A program was designed using Quick Basic language to solve equation (14) by means of which the cumulative line energy (CLE) was calculated with a focus error of (W_{20}) and a spherical aberration of (W_{60}). 20 points were selected on the x and y axes to be sufficient for the purpose of obtaining accurate results even with the existence of aberration. To avoid having the value of zero in the denominator according to equation (14), 24 points were selected on the x_1 axis.

The program was performed and the results for the CLE at several values of z_o for an optimal system were obtained with the existence of focus error as shown in Fig. (2), which displays the distribution of the CLE of an optimal system at different values of focus error. Evident effect of focus error is clear on the CLE, which causes a decrease in the descent of curves as focus error increases.

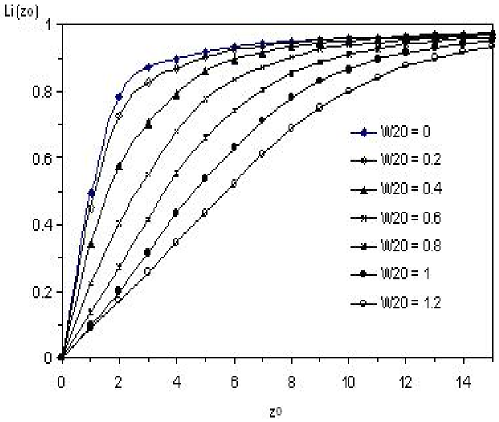

Fig. (2): Distribution of CLE for an optimal system at different values of focal error using a circular aperture

Axial intensity was calculated by graphing the values of the CLE against the focus error for fixed values of z_o as in Fig. (3). In this figure, an increase in the depth of focus was resulted from an increment of z_o due to the increase of the penetrating energy from the slot.

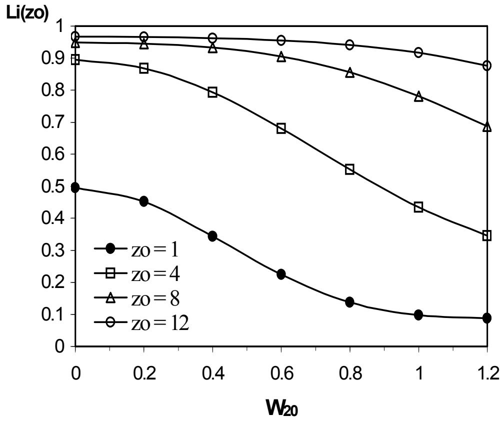

Fig. (3): Normalizing axial intensity of fixed z_o values using circular aperture

Marechal method [9] was used to obtain the best image quality. An accurate compensation was done for aberration indices of different order as shown in Table (1). Solving equation (14) by the compensated aberration values in Table (1), it was possible to get numerical values for the CLE of an optical system of a circular aperture in its optimal condition even with the existence of the secondary spherical aberration (W_{60}) as shown in Fig. (4).

4. Conclusion

A new mathematical model has been derived and solved by means of a numerical integration method using quick basic to find the cumulative line energy (CLE) of an optical system operating with circular aperture with a focal error and spherical aberration. This was carried out to find their effect on the optical system. Accurate balance of aberration coefficient at different values was conducted. It was implemented on the mathematical model and we found that the secondary spherical aberration (W_{60}) has a clear effect on the CLE.

Table (1) Aberration indexes of different order

W_{20}	W_{40}	W_{60}
1.8	− 4.5	3
2.4	− 6	4
3	− 7.5	5
3.6	− 9	6

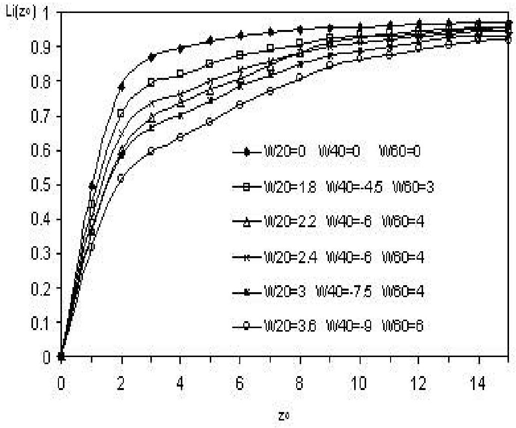

Fig. (4): Comparing CLE values of optical system having secondary spherical aberration in an optimal condition with an optical aberration free system

References

[1] Barakat, R. and Houston, A., *J. Opt. Soc. Am.*, 45 (1964) 786.
[2] Barakat, R. and Houston A., *J. Opt. Soc. Am.*, 55 (1965) 1132.
[3] Tschunko, H.F.A., *Appl. Opt.*, 17 (1978) 1075.
[4] Kirillovskii, V.K. and Krynin L.I., *Sov. J. Opt. Technol.*, 47 (1980) 321.
[5] Friedman E, *Appl. Opt.*, 31 (1992) 14.

[6] Abdulrazak, A.M., “Construction of optical testing system for lens quality evaluation”, Ph.D. Thesis, Al-Mustansiriya University, Baghdad, Iraq (1999).

[7] Hopkins, H.H. and Zalar B., *Modern Optics*, 34 (1987) 371.

[8] Jerri, A.J., “Introduction to integral equation with applications”, Marcel Dekker, Inc. (New York), p.38, 1985.

[9] Marechal, A., *Rev. Opt.*, 26 (1947) 257.

This article was reviewed at The Faculty of Science, Catholic University of America, Washington, U.S.A and Carderock Division, Naval Surface Warfare Center, W. Bethesda, U.S.A

CONFERENCES

ENVIRONMENTAL ELECTROSTATIC 2 - MEASUREMENT METHODS IN ENVIRONMENTAL ELECTROSTATICS

5 July 2006, Institute of Physics, London
Organized by: the Environmental Physics Group of the Institute of Physics
Co-sponsored by: the Electrostatics Group of the Institute of Physics

PLASMA 2006: 5TH INTERNATIONAL SYMPOSIUM ON THE INTRINSIC JOSEPHSON EFFECT IN HIGH TC SUPERCONDUCTORS

17-19 July 2006
Institute of Physics, London, UK
Organised by: the Superconductivity Group of the Institute of Physics and the ESF Arrays of Quantum Dots and Josephson Junctions
Sponsored by: AQDJJ, EPSRC, JSPS, NIMS and the Superconductivity Group

PHOTON06

4 - 7 September 2006
University of Manchester, UK
Organised by: UKCPO and the Institute of Physics
Co-ordinator: Jasmina Bolfek-Radovani

BRSG: 50TH JUBILEE MEETING

5 - 6 September 2006
University of Nottingham, UK
Organised by: the Magnetic Resonance Group of the Institute of Physics

PHYSICAL ACOUSTICS TUTORIAL DAY AND AGM

21 September 2006
Institute of Physics, London, UK
Organised by: Physical Acoustics Group of the Institute of Physics

ENGINEERING AND PHYSICS - SYNERGY FOR SUCCESS

5 October 2006
Institute of Physics, London
Organised by: the Engineering Physics Group of the Institute of Physics
Meetings Co-ordinator: Dawn Stewart

LOW TEMPERATURE TECHNIQUES COURSE

8 November 2006
Aston Business School, Birmingham
Organised by the Low Temperature Group of the Institute of Physics

EXPERIMENTAL TECHNIQUES IN SEMICONDUCTORS RESEARCH

17 November 2006
East Midlands Conference Centre
Organised by the Electron Microscopy and Analysis Group of the Institute of Physics

COMPUTATIONAL MAGNETISM

13 December 2006
Institute of Physics, London, UK
Organised by: the Computational Physics Group of the Institute of Physics

Iraqi J. of Appl. Phys. , Vol. 2 , No. 1-2 , 2006 , 11-15

Walter M. Yokoshvilly*
Yuri V. Believ
Oleg M. Kalimirov

Department of Physics and Astronomy, Belarusian National Academy of Sciences, Minsk, Belarus
* *walteryokoshvilly@hotmail.com*

Effect of the Scattered Solar Radiation on the Atmospheric Ozone Measurements

The spectrometer-ozonometer was used for measurement of radiation at nine wavelengths in the ultraviolet range to register the passed solar radiation. The applicability limits of the Lambert's law for the calculation of atmospheric ozone content by the multi-wavelength method were studied. It was found that the deviations from this law which allow to use the standard method only under solar zenith angles below 80° were due to the light scattering processes. A model proposed in this work made it possible to take into account the light scattering processes, which become important under oblique beam propagation. The model was compared with the calculations on the basis of the multi-wave method. The reflection coefficients for several wavelengths were calculated using the four-flux model.

Keywords: *Solar radiation, Atmospheric measurement, Ozonemetry*

Received: 7 August 2005, Revised: 10 April 2006, Accepted: 20 May 2006

1. Introduction

It is well known that the stratospheric ozone determines the income of the biologically active ultraviolet solar radiation to the Earth's surface. It is a key element in the branched chain of photochemical reactions determining balance of many atmospheric gas constituents [1-2]. Having strong absorption bands in the ultraviolet (UV), infrared (IR), and visible ranges of the solar radiation ozone determines the stratosphere temperature regime. The main ozone mass is located in the middle atmosphere at altitudes of 20–40km. Precisely the middle atmosphere is a connecting link between the troposphere and various manifestation of space activity. Studies of the ozone behavior in the atmosphere presents a considerable interest, in particular from the point of view of the contribution of the energy absorbed by ozone to the atmospheric energy balance. Interacting with various forms of radiant energy the ozone layer may also serve as a model object in the analysis of the radiation propagation through a scattering medium.

In particular, on the basis of ozonometer data one can study the correctness of application of the Lambert's law which most of the ozone content calculation methods from ground-based spectrophotometric measurements are based on [3-4]. This law considers rectilinear propagation of radiation in the scope of the radiant approximation and may be used with high reliability for small solar zenith angles when the main air mass is below the ozone layer and the light is mainly scattered in the lower layers.

Rosenberg [5] showed that the conclusions based on the Lambert's law become incorrect when the atmosphere is illuminated by a diffuse (rather than direct) light flux having approximately uniform angle distribution of the intensity. That is, the scattering processes make impossible application of the existing ozonometric methods just in the twilight. However measurements of the ozone content are of interest in this very period. It is known that the variations of the radiation energetic composition, which impact the ozone content in the atmosphere, occur at sunrise and sunset [6-7]. It will be shown below that the results of ozonometer measurements in twilight are impacted on the first turn by the diffuse component.

2. Experiment

The spectrophotometer-ozonometer constructed on the basis of a double quartz monochromator has been used to register the rectilinear solar radiation intensity in the ultraviolet spectral range [8]. Cloudless days were chosen for the measurements and the registration was carried out during the entire illuminated period of the day with a 5min interval. To determine the total atmospheric ozone content the co-called multi-wave method was used. This method is based on the Lambert's law, which may be written in the form

$$I(\lambda) = I_0(\lambda)\exp(-\alpha\mu(\theta)x - \beta m(\theta) - \delta m'(\theta)) \quad (1)$$

where $I(\lambda)$ is the solar radiation intensity on the Earth's surface; $I_0(\lambda)$ is the intensity of the radiation falling on the upper atmosphere boundary; $\alpha(\lambda)$ is the absorption coefficient of the ultraviolet radiation by ozone molecules; $\beta(\lambda)$ and $\delta(\lambda)$ are the scattering coefficients of the radiation by the air and aerosol; $\mu(\theta)$, $m(\theta)$ and $m'(\theta)$ are the ozone, atmospheric, and aerosol masses, respectively, providing calculation of the oblique ray behavior in the atmosphere, and x is the total ozone content. According to Kuznetsov [4] the multi-wave method is based on the linear equation system obtained from Eq. (1).

The intensity logarithms at nine wavelengths of the absorption spectrum in the Huggins bands were compared. This comparison made it possible to reveal the contribution of the absorption by the ozone molecule lines. Concrete numerical values of the Rayleigh's scattering coefficient calculated for each wavelength [9] were used. The aerosol term .m the contribution of which was studied by Kuznetsov [4] was described according to the assumption on the linear spectral dependence of the aerosol attenuation in a narrow wavelength range. Though a narrow spectral interval is considered the function $\alpha(\lambda)$ varies rather sharply and that makes it possible to evaluate the ozone content in the atmosphere applying the least square method to the system of equations

$$L_{i0} = L_i + \Delta\alpha_i \mu x + \Delta\beta_i m + \Delta\delta_i m' \qquad i = 1,......,8 \quad (2)$$

where $L_i = \ln(I_{0i}/I_{00})$ are the reduced intensities on the Earth's surface, I_{00} is the intensity at a wavelength of 330.6nm which is chosen as a reference one; and L_{i0} are similar intensities outside the atmosphere determined by the Buger-Langly method which was used by many authors [10-11].

3. Theoretical Method

Currently there exist several methods to describe propagation of scattered radiation in various media. They are: the theory of radiative transfer [12], the Kubelka and Munk [13] theory, and so on. The approach developed by Suleymenov and Kuranov [14] is the best to fit the goals of this paper as it enables to describe multiple reflections in arbitrary laminated media (this method is equally applicable to analyze both coherent and incoherent radiation).

Suleymenov and Kuranov [14] showed that each isoplanar layer of the medium may be considered as an effective four-pole (Fig. 1). In particular the atmosphere may be split into layers and for each of them the following relation will be fulfilled

$$\begin{pmatrix} u^- \\ v^- \end{pmatrix} = \begin{pmatrix} a_{11} & a_{21} \\ a_{12} & a_{22} \end{pmatrix} \begin{pmatrix} u^+ \\ v^+ \end{pmatrix} \quad (3)$$

where the radiation fluxes (u^+, v^+) arriving at the chosen layer from the right and from the left are entrance fluxes and the radiation fluxes (u^-, v^-) leaving this layer from both sides are exit fluxes. The diagonal and non-diagonal matrix elements are the transmission coefficients under radiation propagation forward and backwards and reflection coefficients, respectively. It was also shown that a combination of two successive four-poles is described by the matrix

$$A \times B = \frac{1}{1 - a_{12} b_{12}} \begin{pmatrix} a_{11} b_{11} & B a_{12} + b_{12} \\ A b_{21} + a_{21} & a_{22} b_{22} \end{pmatrix} \quad (4)$$

This matrix expresses the composite four-pole parameters via parameters of the initial elements a and b. This operation is as uncommutative as a usual matrix multiplication

$$A \times B \neq B \times A \quad (5)$$

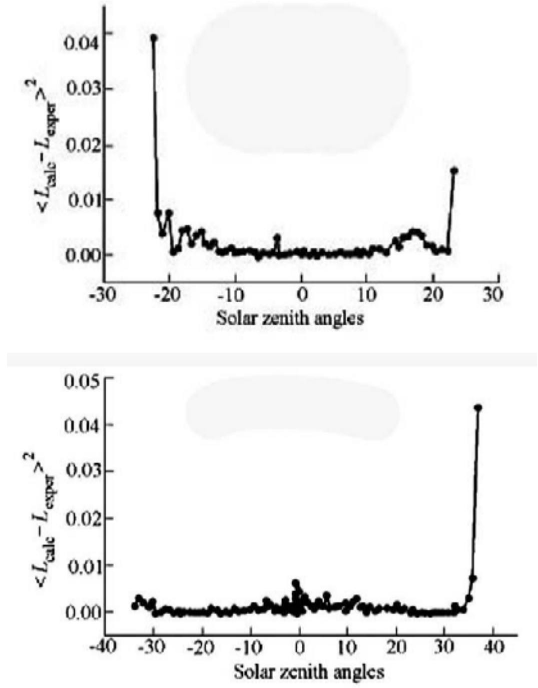

Fig. (1): Dependence of the standard deviations of ozonometric measurements on the solar zenith angle

However if one of these matrices is diagonal then the relation of commutativity is fulfilled.

Using the approximation of light propagation in the above considered system consisting of effective mirrors, the role of the light scattering processes in the ozonometric measurements may be qualitatively interpreted. In this case the atmospheric layers above and below the ozone layer serve as effective partially transmitting mirrors. In respect to the ultraviolet radiation the atmosphere is an analog of a three-mirror interference system in which multiple reflections may occur. The succession of the mirrors corresponds to the layer above the ozone maximum, the ozone layer itself, and the atmosphere above it. Since the ozone layer thickness is negligible as compared with the thickness of the layers above and below, only absorption of the solar ultraviolet radiation occurs and scattering processes in the layer itself may be neglected. In this case the matrix describing the ozone layer is diagonal. The matrices of the other layers are also diagonal if the scattering is neglected. This means that if the light scattering processes in the layer above the ozone maximum are manifested only slightly, then its exact vertical position in the atmosphere plays no role. In this case the A and B matrices may have any order. This situation corresponds to the applicability conditions of the multi-wave method [15]. This condition are broken if the scattering processes above the ozone layer become significant (under large solar zenith angles). In this case one should apply operation (2) to the non-diagonal (and uncommuting) matrices and also establish their particular form. To do that the reflection coefficients of the atmospheric layers above and below the ozone layer due to the Rayleigh scattering should be found.

3. Results and Discussion

Standard deviations $<\Delta L_{calc}-\Delta L_{exp}>^2$ were calculated using series of the 5-minute data of the spectrophotometric measurements obtained during two days (Fig. 2). The values of ΔL_{calc} were calculated on the basis of the Lambert's law using x, μ, and m parameters determined by the standard multi-wave method. Figure 1 shows that approaching θ=75° the calculated intensities begin to differ significantly from the experimental ones.

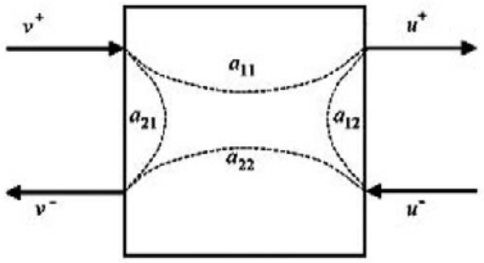

Fig. (2): The light flux transformation by an effective four-pole

The light scattering under large solar zenith angles may be a main process, which can cause the visible deviations from the Lambert's law. It is essential that expression (1) takes into account only the forward light scattering. However the beam pattern of the Rayleigh scattering is symmetric, that is, if the scattering processes play an important role then the backward scattering of the light should be taken into account. Therefore one can suppose that the step-like increase in the errors is due to the backward scattering, that is, to the processes of multiple reflections of the light in the atmosphere.

To calculate the reflection coefficient of an individual layer one can use the four-flux model described by Isimaru [16]. This mo del considers transformation into each other of four different fluxes: the collimated and diffuse downward fluxes, and collimated and diffuse upward fluxes. Figure 3 illustrates the interaction of these fluxes. The left-hand part of Fig. 3 shows schematically that the radiation containing simultaneously both diffuse and collimate components falls on the atmospheric layer from the outside (line A). The figured grey and usual black arrows show conventionally the direction of collimate and diffuse components, respectively. In the similar way the radiation containing both these components may come also from the Earth's surface (line B). The light is scattered within the layer, the collimate component being partially transferred into the diffuse one which can propagate in both directions. The right-hand part of Fig. 3 illustrates in detail the interactions within the layer. Here a thin layer is indicated and the transformation of the downward and upward collimate fluxes into diffuse ones is shown.

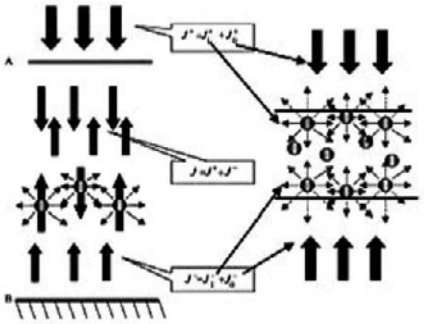

Fig. (3): The Isimaru four-flux model

Figure 3 shows that some part of the radiation in both fluxes is scattered backwards (black dashed arrows). The model described is convenient to use when within the medium there are no pronounced boundaries and absorption processes. In this case the behavior of the diffuse component is governed by the system of two differential equations

$$\frac{d}{dn}\begin{pmatrix} J^+ \\ -J^- \end{pmatrix} = \begin{pmatrix} -\frac{\beta}{2} & \frac{\beta}{2} \\ \frac{\beta}{2} & -\frac{\beta}{2} \end{pmatrix}\begin{pmatrix} J^+ \\ J^- \end{pmatrix} + \frac{\beta}{2}\begin{pmatrix} J_0 \\ J_0 \end{pmatrix} \qquad (6)$$

where β is the Rayleigh scattering coefficient (multiplier 1/2 assumes that the scattered radiation provides the same contribution to oppositely directed fluxes), J^+ and J^- are the intensities of the downward and upward light fluxes, respectively, and J_0 is the intensity of the downward collimate flux. In Eq. (2), the collimate component transformed to the diffuse one because of light scattering plays the role of a "source". Summing and subtracting Eq. (6) we obtain equations for the integral light intensity $J=(J^++J^-)$ and direct diffuse light flux (J^+-J^-)

$$\frac{d}{dn}\begin{pmatrix} J^+-J^- \\ J^++J^- \end{pmatrix} = \begin{pmatrix} 0 & 0 \\ -\beta & 0 \end{pmatrix}\begin{pmatrix} J^+-J^- \\ J^++J^- \end{pmatrix} + \beta\begin{pmatrix} J_0 \\ 0 \end{pmatrix} \qquad (7)$$

which is reduced to the only diffuse equation with a source in the right-hand side

$$\frac{d^2J}{dh^2} = -\beta^2 J_0 \qquad (8)$$

Here the vertical distribution of the collimate component is governed by the usual Lambert's law

$$J_0 = J_{00}\exp(-\beta h) \qquad (9)$$

Taking into account Eq. (5) the general solution of Eq. (4) has the form

$$J = J_0\exp(-\beta h) + C_1 + C_2 h \qquad (10)$$

The main feature of the problem in question is that the boundary conditions are set up on the values of the upward and downward fluxes but not on the values of the integral intensity, which fits Eq. (4). In other words, the value of the downward flux at the upper boundary of J_0^+ (we choose this point as the origin of the frame of reference with the h axis directed downward) may be considered as a given value. In a similar manner the condition of the complete absorption by the Earth's surface (point h_m) is expressed by $J\,\big|_{hm}=0$. The values of the upward and downward fluxes may be expressed via the distribution of the integral intensity and its derivative according to (3) and (4)

$$J^+ = \frac{J\beta - J'}{2\beta} \qquad (11)$$

$$J^- = \frac{J\beta + J'}{2\beta} \qquad (12)$$

Using Eq.'s (7) and (8) and taking into account the boundary conditions one can obtain the expression for the upward component:

$$J^- = (J_{00} + J_0^+)\frac{\beta(h_m - h)}{\beta h_m + 2} \qquad (13)$$

One can see that the values of the downward fluxes (both diffuse and collimate components) enter in a similar way the expression obtained. Therefore one can determine the reflection coefficient which according to Eq. (9) will be

$$r = \frac{\beta(h_m - h)}{\beta h_m + 2} \qquad (14)$$

For the case of oblique incidence the same equation may be expressed in terms of the scattering coefficient referred to the entire thickness of the layer considered $\beta_0=\beta h_m$

$$r = \frac{\beta_0}{\beta_0 + 2\cos\theta} \qquad (15)$$

Figure 4 shows an example of the calculated dependence of the reflection coefficient on the solar zenith angle in the range typical for middle latitudes. One can see that from noon to twilight this value increases by several times and that indicates once again to an increasing role of scattering processes in twilight.

For the beginning we note that if the light scattering processes are essential only in the atmospheric layers below the ozone layer then they almost do not impact the results obtained by the multi-wave method [15]. This is because the measurements are conducted in a narrow enough spectral range. On the contrary, the multi-wave method becomes inapplicable if scattering processes are essential in the atmosphere including the atmospheric layers above the ozone layer. We compare the calculation results obtained with the help of the multi-wave method and on the basis of the theoretical considerations described above. The operation (4) may be done assuming that the total air content above the ozone layer is about 5% of the its total mass and using the reflection coefficient (15) to determine the elements of matrix (3). This leads to the following expression for the transmission factor of the three-layer atmosphere

$$T = \frac{\exp(-\alpha x/\cos\theta)}{1 + \beta/\cos\theta + 0.05(1 - \exp(1 - \exp(-2\alpha x/\cos\theta))(\beta^2/\cos^2\theta)} \qquad (16)$$

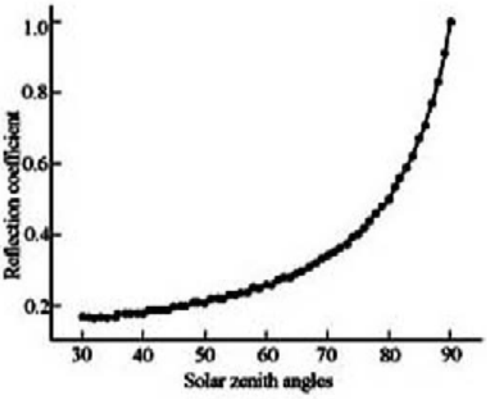

Fig. (4): Dependence of the reflection coefficient on the solar zenith angle

On the basis of Eq. (16) the standard deviation $<L_{new}-L_{lamb}>^2$ was calculated as a function of the solar zenith angle (Fig. 5, curve 1). Here $L_{new}=log(I/I_0)=log(T)$ and L_{lamb} was calculated using the multi-wave method. Real atmospheric parameters were used for the days shown in Fig. 1. Figure 5 shows graphs based on the data in Fig. 1 but presented in a more convenient scale for comparison (curve 2). One can see that the calculations performed for the model three-mirror system also indicate to the existence of the critical zenith angles at which the standard deviation increases abruptly. That means that precisely the atmospheric scattering processes above the ozone layer are responsible for their existence.

4. Conclusion

It is shown that at large solar zenith angles the standard deviations given by the known multi-wave method increase abruptly. The analysis of the causes of these errors carried out with the help of the optical methods of the laminated medium theory makes it possible to establish that under certain conditions the terrestrial atmosphere presents an analog of a three-mirror interference system and the atmospheric layers serve as partially transmitting mirrors for the ultraviolet radiation in the Huggins band. The essential role played by the radiation diffuse component at large solar zenith angles is established. Using the four-flux model specific equations for calculations of the reflection coefficients of the atmospheric layers determined by processes of the backward light scattering are obtained. A mathematical description of the radiation propagation through a layer structure is proposed, the description taking into account mutual transformation of diffuse and collimate light components. Thus the results obtained in the paper spread outside the framework of the ozonometry. For instance, they can be used to study the energetic balance of the ozone layer during the dawn-dusk hours. Actually, since the reflection from the effective mirrors above and below the ozone layer in the twilight becomes significant, the radiation may be quite "captured" between them. Hence there follows a possibility of occurrence of significant disturbances of the ozone layer in the twilight. The results obtained make it also possible to suggest that studies of light reflection processes from atmospheric layers may appear important for the analysis of interactions between atmospheric components and radiation in other spectral ranges.

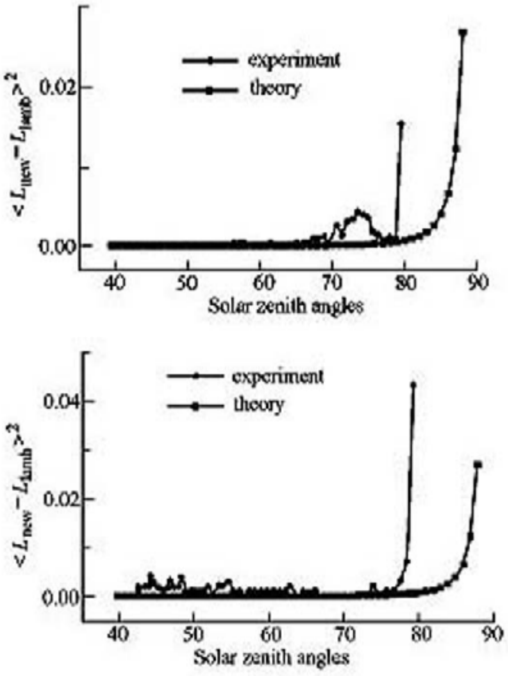

Fig. (5): Comparison of the experimental and theoretical results

References

[1] Hesstvedt, E., *Ann. Int. Geophys.*, 21(1) (1969) 99.
[2] Hunt, B. G., *J. Geophys. Res.*, 71(5) (1966) 1385.
[3] Dobson, G., *Ann. Int. Geophys.*, 5 (1957) 46.
[4] Kuznetsov, G.I., *Izv. Akad. Nauk SSSR Fiz. Atmos. Okeana* (in Russian), 11(6) (1975) 647.
[5] Rosenberg, G.V., "**Twilight**", Plenum Press (New York) (1966) 358.
[6] Pearce, F., *New Sci.*, 153 (1997) 2067.
[7] Randhawa J.S., A Balloon Measurement of Ozone Near Sunrise, Atmos. Sci. Lab. White Sands Missile Range (N.Y.) (1970), 27.
[8] Bekturganov, B.K., Ivanov, A.I. and Korovchenko, V.N., The spectrophotometer-ozonometer on the basis of double quartz monochromator DMR 4, in Some Questions of Solid Physics and Optics (in Russian), Nauka, Alma-Ata (1982) 12–18.
[9] Vigrougx, E., *Ann. Geophys.*, 2(4) (1967) 209.
[10] Fraser, J., *J. Appl. Meteorol.*, 14 (1187) 1975.
[11] Shaw, G., *J. Appl. Meteorol.*, 18 (1979) 1335.
[12] Chandrosekhar, S., "**Radiative Transfer**", Oxford University Press (London) (1950).
[13] Kubelka, P. and Munk, F., *Zs. Tech. Phys.*, 12 (1931) 593.
[14] Suleymenov, I.E. and Kuranov, A.L., *Optika Spektroskopiya* (in Russian), 82(3) (1997) 484.
[15] Zyryanova, O., Suleymenov, I. and Somsikov, V., *Izv. Akad. Nauk Kazak.* (in Russian), 4 (1998) 186.
[16] Isimaru, A., "**Wave Propagation and Scattering in Random Media**", Academic Press (N.Y.) (1978).

This article was reviewed at The Department of Physics and Astronomy, Schuster Laboratory, Manchester University, UK and The School of Applied Sciences, University of Technology, Baghdad, IRAQ

ICNMTA 2006

10TH INTERNATIONAL CONFERENCE ON NUCLEAR MICROPROBE TECHNOLOGY AND APPLICATIONS

Date: 9 - 14 July 2006
Venue: Shangri-la Rasa Sentosa Resort, Singapore
Website: http://www.icnmta2006.org/index.html

MEGAGAUSS XI

MG-XI is the 11th International Conference on Ultra High Magnetic Fields: their Science, Technology and Application.
Date: 10 - 14 September 2006 , Imperial College, London, UK
Website: http://conferences.iee.org/MG-XI
Email: ejarvis@theiet.org

THE EGYPTIAN MATERIALS RESEARCH SOCIETY (EG-MRS)

organizes in cooparation with Arab Academy for Science, Technology & Maritime Transport

EG-MRS 2006

THE XXVI CONFERENCE

SOLID STATE PHYSICS AND MATERIALS SCIENCE

WORKSHOP

NANOSTRUCTURES: SCIENCE, FABRICATION, CHARACTERIZATION AND DEVICES

SEMINAR

Pre-University Science Education

10 -14 September 2006
Alexandria, Egypt
Call for Abstracts and Registration

THE CONFERENCE IS HELD UNDER THE AUSPICES OF

Prof. Dr. Yousry El-Gamal,
Minister of Education
Prof. Dr. Gamal Mokhtar,
President, Arab Academy for Science, Technology & Maritime Transport, Honorary Chairmanship
Prof. Dr. Raafat K. Wasef,
Cairo University
Prof. Dr. Omar Abd El-Aziz,
Arab Academy for Science, Technology & Maritime Transport

BOARD

Conference Chairman:
Prof. Dr. Kamal Abd El-Hady (Minia Univ.)
Conference Co-Chairman:
Prof. Dr. Fakhry Abd El-Salam (Ain Shams Univ.)
Prof. Dr. Abdelrazek Y. Kandeil (AASTMT)
Workshop International Organizer:
Prof. Dr. Hanns-Ulrich Habermeier
(Max-Planck-Institute, Stuttgart)
***Workshop Chairman*:**
Prof. Dr. M. Hassan Talaat (Ain Shams Univ.)
Workshop Co-Chairman:
Prof. Dr. Ahmed A. Ramadan (Helwan Univ.)
Organizing Committee:
Prof. Dr. Fayez Shahin (Beni-Suef Univ.)
Prof. Dr. Hassan Afify (NRC, Cairo)
Prof. Dr. Hesham M. Talaat (Al-Azhar Univ.)
Prof. Dr. Mohamed El-Okr (Al-Azhar Univ.)
Prof. Dr. Sherif A. Khairy (Cairo Univ.)
Local Organizing Committee:
Eng. Mahmoud Morsi (AASTMT)
Dr. Fathi Ibrahim (AASTMT)
Dr. Moataz Soliman (ASMS)
Dr. Osama El-Shazly (Alexandria Univ.)
All correspondences should be addressed to:

MAILING ADDRESS
Egyptian Materials Research Society (Eg-MRS),
33 Abdel-Khalik Tharwat Street, Cairo, Egypt.
Telephone/Fax: +202-3925997
(Sunday & Wednesday, 6-10 pm)
E-mail: contact@egmrs.org
Web: http: //www.egmrs.org

Iraqi J. of Appl. Phys. , Vol. 2 , No. 1-2 , 2006 , 17-21

Sergey I. Vlaskina

Institute of Semiconductor
Physics, NAS of Ukraine,
Kyiv, Ukraine
businkaa@mail.ru

Characteristics of p-n Junction Silicon Carbide LED

Silicon carbide has been widely used as material for manufacturing yellow, red, green LED and optoelecronics devices (indicators, screens). The silicon carbide LED technology has been investigated for improvement of their operational characteristics. This includes the influences of the surface processing (etching, annealing), the formation method for the p-n junctions and the contacts on the LED properties. Light-emitting devices used as light sources for optical-fiber communication lines. LED fabricated by Al^+ ion-implanted in 6H-SiC and investigated their characteristics for an effective green LED. The brightness of the ion-implanted p-n junction was found to be two orders higher than that of diffusion p-n junction, and the best value was 2000-10000 cd/m^2 with passing current about 0.5mA through area 50x50μm and applied voltage about 2.6±0.2V. The ion-implanted structures showed a high stability of light in the temperature range of 77-600K.

Keywords: *Silicon carbide, LED, Ion implantation*

Received: 1 February 2006, Revised: 8 April 2006, Accepted: 30 April 2006

1. Introduction

Silicon carbide LED first became a significant commercial success when ÑREE (USA) got them on the market in the early 1990's. Today, CREE's CB series of super bright LED are a new generation of solid-state LED emitters, which combine highly efficient InGaN with CREE's SiC substrate. CREE's main LED products now have SiC as a substrate for gallium nitride or indium gallium nitride as active ingredients, and emit blue as well as green and blue-green luminescence. Yellow silicon carbide LED's had been made around 1970-1975 in the former Soviet Union. Diffusion p-n junctions had been applied to manufacturing this LED devices. Single crystalline SiC with $N_D x N_A=(1\sim5)x10^{18}cm^{-3}$ was suitable for manufacturing such devices. The diffusion factors depend on the concentrations of the impurities in the crystals. The process of p-n junction creation is rather complicated because the usual impurity concentrations in crystals range from 10^{17} to 10^{18} cm^{-3}. The optimal depth (1μm) of the p-n junction had been obtained with industrial crystals [1].

To obtain a high manufacturing yield for LED with uniform light, the following technique had been applied. Diffusion of Al with O was carried out for 2 hr at 1700°C. Then, B and Al were introduced for 15 min at 1600°C. The sources for O, Al, and B were SiO, 99.99% Al and B_2O_3, respectively. After the diffusion processes, appreciable changes in the surface morphology or the carbon traces were observed using optical microscopy. The low-temperature (77K) and the high-temperature (300K) photoluminescence in the ultraviolet wavelength range showed repeatable and clear spectra for the uniformly doped samples. Diffusion of Al and O above 1700°C resulted in a deterioration of the surface conditions, and diffusion of B and Al at higher temperatures made the photoluminescence spectra less clear and the surface conditions even worse. The time at optimum temperature could be adjusted to change the color of electro-luminescence from yellow-green to red (in the wavelength range between 5600Å and 6000Å). In the case of a yellow-green color (5600Å), the time for the diffusion of B and Al turned out to be 20-25min. A further increase in the diffusion time caused the p-n junction to be less sharp as well as the voltage drop on the p-layer to increase, and, consequently, spreading of the current carriers on the p-layer and less clear light drawings on the displays. At the shortest diffusion time (5min) for B and Al, the thickness of the p-n junction was too small to assure an effective LED. The parameters of such LED and indicators, which had been fabricated, are listed in Table 1. Usage of another SiC polytypes (4H, 3C, 15R) allows to change the color of light, too.

Because of the extreme stability of silicon carbide, it is not necessary to dope the crystal by thermal diffusion. Instead, dopants can be introduced by ion implantation. Once implanted into the crystal, the dopant atoms occupy interstitial positions in the lattice and must be transferred to substitution sites to become electrically active. This "activation" is accomplished by high temperature annealing in an inert ambient such as argon. Nitrogen and phosphorous are typical n-type dopants in SiC.

Table (1) LED (diffusion p-n junction) on 6H-SiC

Device	Light voltage (V)	Light current (mA)	Working voltage (V)	Brightness (cd/m^2)	Size of light area (μm^2)
LED indicator (10 elements)	2.2	5	2.4±0.2	30-80	800x300
LED matrix (64 elements)	2.5±0.1	0.5	3.0±0.2	60	120x120 step 100
LED break with high resolution (64 elements)	2.4±0.2	2.5	3.1±0.1	70	40x40 step 60
LED break (100 elements)	2.4±0.2	0.5	2.8±0.1	80	100x100 step 100
LED break with face conclusion of light (step 100)					40x40 step 60

Aluminum and boron are p-type dopants. Implantation is usually conducted with the sample at elevated temperatures (600-800°C) to provide some in-situ annealing of lattice damages caused by the implant. The implanted sample is subsequently annealed at temperatures 1000-1700°C for times 5 and 90 minutes to activate the dopants. The dynamics of activation depends both on the dopant species (i.e. aluminum and boron, nitrogen and phosphorus) and upon the SiC polytype (i.e., 4H or 6H). Activation of nitrogen implants in 4H-SiC requires higher annealing temperatures than those in 6H-SiC. Phosphorus is an excellent n-type dopant in 4H-SiC when implanted at high doses, such as for source and drain regions of MOSFET p-type dopants, aluminium and boron, require much higher temperatures for efficient activation and temperatures above of 1650°C are necessary for that. Aluminum implants typically achieve the same degree of activation at annealing temperatures about 100°C lower than boron. At any given annealing temperature, there exists an optimum annealing time [2].

This article reports results of SiC green LED electrical characterization. This LED had the same brightness as CREE's LED, but higher stability, more simple design (without AlGaN or GaN layers) and can be used in various usual applications.

2. Experiment

Green LED had been prepared by the method of ionimplantation of impurities into 6H-SiC crystals. Al^+-implanted for p-n junctions in 6H-SiC substrates and their characteristics were investigated as an effective LED. The ion-implantation was carried out on polished n-type 6HSiC crystals and on epitaxial layers of 6H-SiC with an impurity concentration of $N_D x N_A = (2\text{-}8) \times 10^{18}$ cm^{-3}. Substrate was doped by donor nitrogen. Implantation was performed with 80keV Al^+ by using an ion accelerator. The implanted depth was 0.5μm, and the concentration of Al was 10^{20} cm^{-3}. The optimum implantation time and the substrate temperature were 2 min and 660°C, respectively.

Despite the low resistance of the p-layers, a thin high resistive layer of C was formed on the surface of the crystals after implantation. This C film reduced the adhesion of the metals deposited for the contacts, increased the resistance of the contacts to the p-layers, and worsened the light uniformity. The crystals were annealed at 800-1100°C for 2-10 min to remove the C layer and to reduce the quantities of radioactive defects. Before the LED fabrication process, the crystals were etched in an acid mixture of HF and HNO_3.

Contacts were prepared by deposition of Al layer on p-SiC heated to the temperature 550°C in vacuum (implanted and annealed). Al contact thickness was less or about 4000Å. Ni layers was deposited for protection of Al layer from oxidation and for better contact with wire during LED manufacturing. Thickness of Ni layer was about 2000Å. Contacts to the n-SiC substrate were made by laser using Ti and Ni wire. Contact of necessary configuration were made by photolithography methods.

3. Results and Discussion

Photos of prepared LED are shown in Fig.1 (a, b, c). Just this LED was made on n-epitaxial layer grown by Tairov's method. The boundary between n-layer and implanted p-layer is shown. The block structure of epilayer and p-n junction is also shown. Single crystals grown by the Lely method had been used for such LEDs, too, but photos of epilayers with implanted aluminum are more interesting than these of single crystals with p-n junction. The voltage-current characteristics of ion-implanted p-n junctions are shown in Fig. 2. The differential degree $\alpha = dl_g I/dV$ is shown in Fig. 3.

In the low voltage area (at a voltages less then 0.08V), α is about unity. Determined from this linear site leakage is $(1\text{-}2) \times 10^4 \Omega$. The reason of such resistance is carbon or silicon oxide on the surface of LED. In the region of very small voltages:

$$I = I_0 \exp\left(\frac{V}{V_T}\right) \qquad (1)$$

This circumstance, as well as independence of V_T on temperature permits to think about tunnel character of this part of the voltage-current characteristics. Concentration evaluated from a volume charge is as follows:

$$N = \frac{1}{e}\left|\int_{n_s}^{n_n}\frac{\rho(n)}{n}dn\right| = \frac{\pi^2 \varepsilon m}{32h^2}V_T^2 \qquad (2)$$

N about (1-4)x10^{20}cm^{-3} is indicative of a rather high doping level of the junction. The ideality factor 1.9 to 3.2 was obtained from the following exponential part of the forward bias current-voltage characteristics. The forward saturation current was (3-5)x10^{-16} to (3-5)x10^{-8} A/cm^2 and forward turn-on voltage of 0.8 to 2V (at current density about (5-8)x10^{-8} A/cm^2. Reverse biasing produced average leakage currents were that were of the order of 10^{-8} to 10^{-3} A/cm^2 (at 10 to 20V reverse bias).

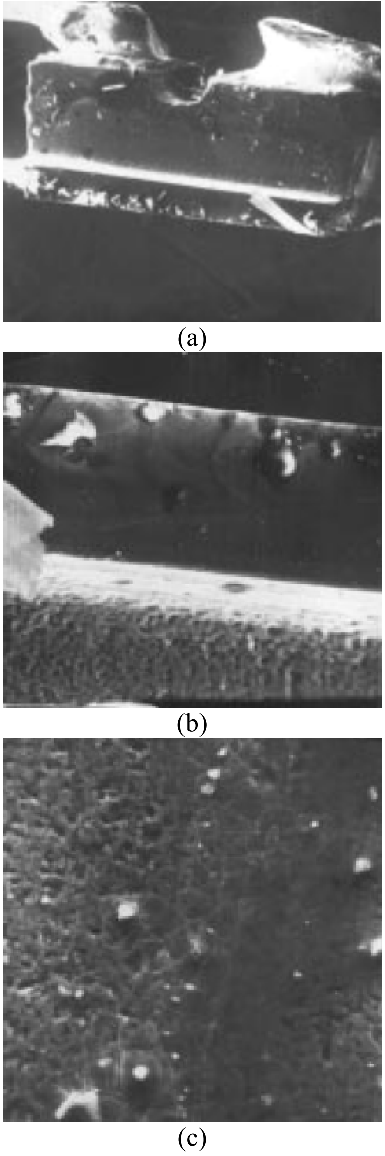
(a)
(b)
(c)

Fig. (1): Micro photo of ion-implanted LED: Magnitude: (a) x75, (b) x380, (c) x730

The ideality factor had some trends. Namely, the ideality factor is decreased and forward current density is increased with increasing operation temperature in the range of 20°C to 400°C. The ideality factor is of the order of 2 for most LED suggesting that recombination/generation current is dominant over diffusion current. The ion-implanted p-n junctions are sharp, and the injection of carriers as well as their recombination in the player prevail. The sharpness was maintained in the temperature range between 77K and 500K. Recombination happens in the layer of the volume charge in the p-n junction at low levels of injection, but the recombination prevails in either the p- or the n-area at high levels of injection, depending on the doping degree.

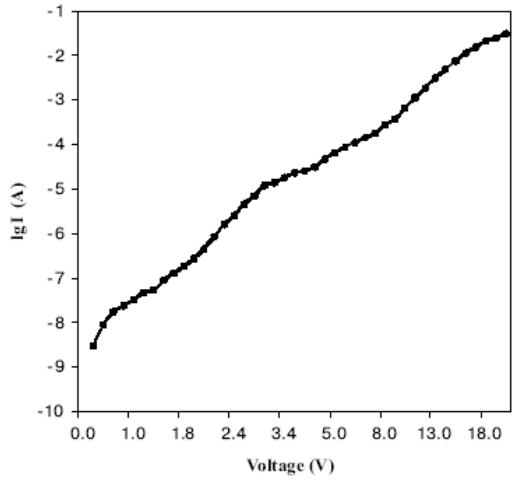

Fig. (2): Voltage-current characteristics of ion-implanted p-n junction in 6H-SiC

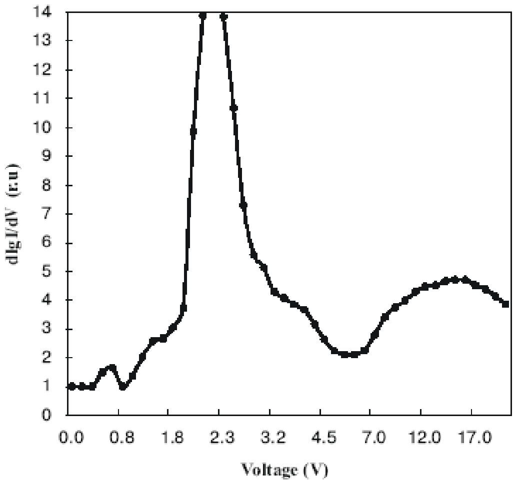

Fig. (3): Derivation from voltage-current characteristics of ion-implanted LED

In the region of voltages changing from 2.2V to 18V the α degree is reduced passing the flat minimum. Then α degree (Figs 2, 3) is again increased and can be described by the expression:

$$V = \left\{\begin{matrix} AI^{\frac{1}{2}} + V_0 \\ BI^{\frac{1}{4}} + V_\infty \end{matrix}\right\} \qquad (3)$$

The square-law part of the voltage-current characteristics enables to calculate the major carrier lifetime near the cathode:

$$\tau_{n_k} = \frac{L^2}{2\mu V_0} = (0.8-1.2)\times 10^{-8}s \qquad (4)$$

(μn=100cm^2/V$_s$)

That is in good agreement with the experimental data of transitive characteristics, where ignition time is (2.5-3)x10^{-8}s and emission time is (1-1.5)x10^{-8}s. The light-brightness characteristic of the ion-implanted p-n junction is shown in Fig. 4. The differential degree $\beta=dB/dl_gI$ is shown in Fig. 5. The linear region extends from 7x10^{-4}A to 10^{-2}A/cm^2. The high stability of the light, even at 77-600K, is another characteristic for the ion-implanted structures, which is understood mainly by the role of the radioactive defects in the emission. The concentration of defects is constant in the temperature range of 77-600K.

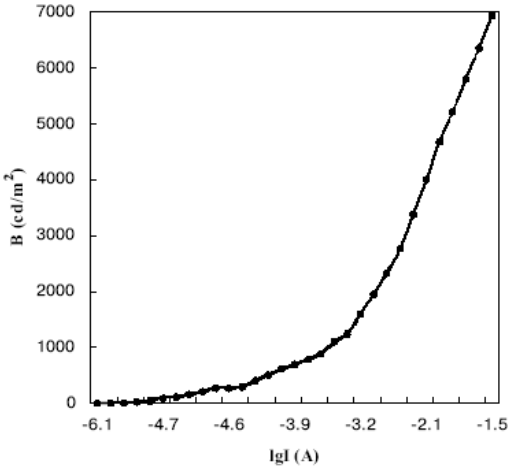

Fig. (4): Ion-implanted p-n junction light brightness characteristics

The destructive features of the ion-implanted structures produced narrow lines in the electro-luminescence spectra at relatively small current (Fig. 6) A correlation between the narrow lines in the spectra and the brightness of LED had been established; most of the effective LED had narrow lines at low temperatures. It is a very convenient way to select crystals for green highly bright LED. When the temperature increases, the narrow lines disappear from the spectra. The fact that the sharp-line structures of the electro-luminescence spectra coincide with those of the photoluminescence spectra at low temperatures (77K) is an additional indication to support the suggestion that the characteristics of the spectra are due to radioactive defects.

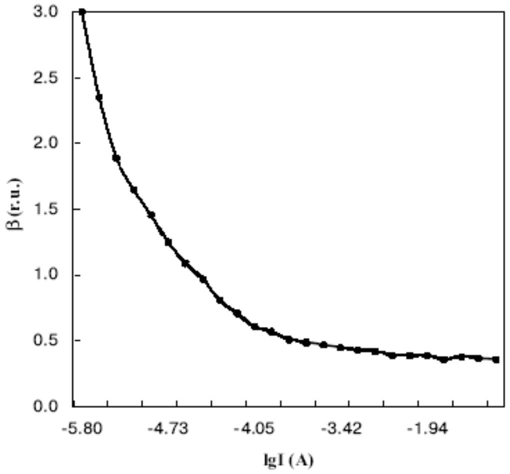

Fig. (5): Derivation from brightness-current characteristics of ion-implanted p-n junction

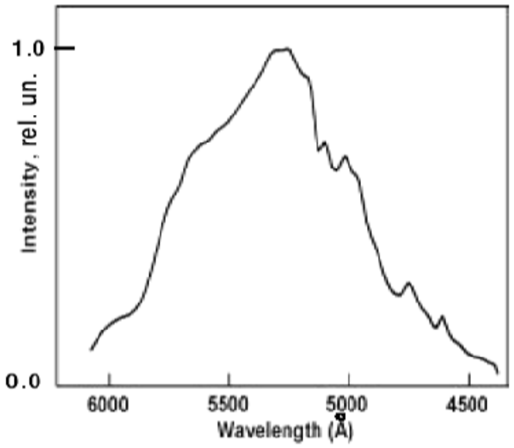

Fig. (6): Ion-implanted p-n junction electroluminescence spectrum

The ion-implanted structures have much faster response times than the diffused ones (Table 2). The switching time is close to 10^{-8}s, which provides wide opportunities for the applications of such LED to optical couples and optical-fiber communication lines. The brightness of the diffused LED is 30-100 cd/m^2 at 10mA/mm^2, while for the ion-implanted it is 500-600 cd/m^2 at 10mA/mm^2 and even (2-10)x1000 cd/m^2 for the best samples. On the other hand, ion-implanted p-n junctions can be applied widely in optical-fiber communication, especially, short communication lines, because of their high speed (10^{-8}s), high stability of light for 10,000 hrs, linear brightness-current characteristics up to a current density of 10A/cm^2, high brightness, absence of brightness degradation, and stability of characteristics over a wide interval of temperatures.

Table (2) LED for the fiber communication line

Switching voltage (V)	Switching current (mA)	Working voltage (V)	Brightness (cd/m^2)	Size of light area (µm^2)	Switching time (s)
2.6±0.2	0.5	3.2±0.1	2000-4000	50x50	0.15
				80x50	0.1

4. Conclusion

The characteristics of silicon carbide LEDs were investigated. These included the influence of surface processing, the formation method of the p-n junctions, and the contacts on the properties of the LED. Green SiC LEDs can be used as light sources for optical-fiber communication lines, in the traffic lights, as indicators, in screens and so on. p-n junctions were fabricated by Al^+ ion-implantation 6H-SiC, and annealed at 800-1100°C. Characteristics for using as effective green LED had been investigated. The brightness of the best ion-implanted p-n junction was found to be about 2000-10000 cd/m^2. The ion-implanted structures showed a high stability of light in the temperature range of 77-600K. The pulsing characteristics of these LEDs based on ion-implanted structures had a response time close to 10^{-8}s.

References

[1] Vlaskina, S.I. *et al.*, Optoelectronics Devices on Silicon Carbide, J. Korean Phys. Soc., 30(1) (1997) 117-121.

[2] Capano, M.A., Santhakumar, R., Cooper, Ir., J.A. and Meloch, M.R., SiC Ion Implantation Research at Purdue, USA (internet information), 2002.

This article was reviewed at The Department of Electrical and Computer Engineering, National Technical University of Athens, Greece

---

The 5th International Conference on Atomic and Molecular Data and Their Applications (ICAMDATA)
Meudon, France
October 15-19, 2006

We cordially invite you to attend the Fifth International Conference on Atomic and Molecular Data and Their Applications (ICAMDATA) that will be held October 15-19, 2006 in Meudon, France at the observatory of Paris.

Topics covered by the conference include atomic and molecular data production, collection, assessment, and dissemination, laboratory data needs and applications, astrophysical and atmospheric applications, inertial and magnetic fusion, lighting, plasma processing, and other similar applications relying on understanding of atomic and molecular processes and needing atomic and molecular data.

Deadline for abstract submission : September 17th

CONFERENCES

14th International School on Quantum Electronics: Lasers-Physics and Applications
18 - 22 September 2006 , Sunny Beach, Bulgaria , Sponsored by SPIE Bulgaria Chapter. SPIE will publish proceedings.

Photomask Technology, 26th Annual Symposium
18 - 22 September 2006 , Monterey, California USA , Advance Registration Ends 5 September 2006 , Exhibition

Boulder Damage Symposium
25 - 27 September 2006 , Boulder, Colorado USA , Abstracts Due 5 June 2006

Optical Imaging 2006, *Fifth Inter-Institute Workshop on*
Optical Diagnostic Imaging from Bench to Bedside at the National Institutes of Health
25 - 27 September 2006 , Bethesda, Maryland USA , *Organized by SPIE.* Abstracts Due 30 June 2006

SPIE Optics East
1 - 4 October 2006 , Boston, Massachusetts USA , Advance Registration Ends 21 September 2006 , Exhibition

Advanced Study Institute
Optical Waveguide Sensing & Imaging in Medicine, Environment, Security and Defense
12 - 21 October 2006 , Gatineau Québec, Canada

International Optical Fiber Sensors Conference (OFS 18)
23 - 27 October 2006 , Cancun, Mexico , SPIE is a technical co-sponsor

SPIE Asia-Pacific Remote Sensing
13 - 17 November 2006 , Goa, India , Abstracts Due 3 July 2006

5th International Conference on Optics-photonics Design & Fabrication (ODF'06)
6 - 8 December 2006 , Nara, Japan , SPIE is a cooperating organization

SPIE Microelectronics, MEMS, and Nanotechnology
10 - 13 December 2006 , Adelaide, Australia , Abstracts Due 5 June 2006

Photonics India 2006
13 - 16 December 2006 , Hyderabad, India , SPIE is a technical co-sponsor

International Conference on Computers and Devices for Communication (CODEC 2006)
18 - 21 December 2006 , Kolkata, India , SPIE is a cooperating organization

UPCOMING IN 2007

SPIE PHOTONICS WEST
20 - 25 January 2007 San Jose, California USA
Abstracts Due 10 July 2006 , Exhibition

IS&T/SPIE ELECTRONIC IMAGING
28 January - 1 February 2007 San Jose, CA USA
Abstracts Due 17 July 2006

SPIE MEDICAL IMAGING
17 - 22 February 2007 San Diego, CA USA
Abstracts Due 7 August 2006

SPIE ADVANCED LITHOGRAPHY (FORMERLY MICROLITHOGRAPHY)
25 February - 2 March 2007 San Jose, California USA
Abstracts Due 14 August 2006

SPIE SMART STRUCTURES & MATERIALS/NDE
18 - 22 March 2007 San Diego, California USA
Abstracts Due 4 September 2006

SPIE DEFENSE AND SECURITY SYMPOSIUM
9 - 13 April 2007 Orlando, Florida USA

PHOTOMASK JAPAN 2007
17 - 19 April 2007 Yokohama, Japan
Abstracts will be accepted beginning on 20 October

SPIE OPTIFAB
14 - 17 May 2007 Rochester, New York USA
Abstracts Due 25 September 2007 , Exhibition

OPTICAL DATA STORAGE
21 - 24 May 2007 Portland, Oregon USA
Co-Sponsored by OSA, SPIE, and IEEE-LEOS

XXTH JOINT SYMPOSIUM ON PHOTONICS AND ELECTRONICS FOR ACCELERATORS AND HIGH ENERGY PHYSICS EXPERIMENTS
21 - 27 May 2007 Wilga, Poland
SPIE Poland Chapter is a co-sponsor

8TH INTERNATIONAL CONFERENCE ON QUALITY CONTROL BY ARTIFICIAL VISION QCAV 2007
23 - 25 May 2007 Le Creusot, France
SPIE Europe is a cooperating organization

INTERNATIONAL CONFERENCE ON SMART MATERIALS AND NANOTECHNOLOGY IN ENGINEERING
1 - 4 July 2007 , Harbin, China (*SPIE co-organization)*
Abstracts Due 28 October 2006

SPIE OPTICS & PHOTONICS
26 - 31 August 2007 San Diego, California USA

SPIE OPTICS EAST
7 - 14 September 2007 Boston, Massachusetts USA

Salwan K.J. Al-Ani[1]
Subhi S. Al-Rawi[2]
Ayad H. Jassim[2]
Haifaa A. Al-Hilli[2]

[1] *Faculty of Education, Seyoun-Hadhramout University for Science and Technology, Yemen, salwan_kamal@yahoo.com*
[2] *Department of Physics, College of Science, University of Baghdad, Baghdad, IRAQ*

FTIR Spectra of Molybdenum Tellurite Glasses

A series of binary tellurite glasses in the form $TeO_{2(100-x)}$ - $MoO_{3(x)}$ when [x=10, 20, 30, 40, 50, 55wt%] were prepared. FTIR spectra were measured in the range (4000-200) cm^{-1} and (2000-200) cm^{-1} respectively. The peak positions were measured and correlated to the composition and structure of the glasses .Results were compared with the crystalline states of TeO_2. The FTIR spectra of these glass systems indicate that the modified oxides are connected to the chains of TeO_4 units.

Keywords: *Te glasses, $TeO_{2(100-x)}$-$MoO_{3(x)}$, FTIR spectra, crystalline TeO_2*

Received: 31 January 2006, Revised: 22 March 2006, Accepted: 5 April 2006

1. Introduction

Tellurite glasses are relatively new class of vitreous material, having gained popularity as a result of pioneer work by Stenworth [1]. It is well known that pure TeO_2 is vitrified with difficulty [2-3] and there was considerable doubt about the existence of TeO_2 in a true glassy state. TeO_2 glass was, however, prepared and its optical absorption and infrared in tungsten tellurite glasses was studied [4].

Tellurite glasses with TeO_2 as the main former are considered as potential candidate materials for all optical switching materials and laser host. They are of technical interest on account of their low melting points, high refractive indices, dielectric constants, good infrared transmissions, and high thermal expansion coefficients [5].

The structure of amorphous TeO_2 and other tellurite glasses has been the subject of several investigation [2,6]. TeO_2 glasses have been reported to consist of a network of individual interconnected deformed TeO_4 trigonal bipyramids with two equatorial and two axial bonds leaving alone pair of electrons in the equatorial position. This building unit of TeO_4 is then connected to the neighboring units via bridging oxygen to form three dimensional crystalline structure. In tellurite glasses, however, the modifier atoms play one more important role that is causing the variation of the structural unit itself. Structural units of tellurite glasses are reported to be TeO_X (x=3-6) polyhedra [7-8]. It is in contrast with the structural unit of silicate glasses (SiO_4 tetrahedron) which is not affected by modifier atoms. Dimitrieve *et. al* [6] have studied the short range order of TeO_2-V_2O_5 and TeO_2-MoO_3 glasses using infrared spectroscopy by comparing the infrared spectra recorded from both amorphous and crystalline materials, they suggest that transition of TeO_4-TeO_3 took place within basic structural units with the introduction V_2O_5 and MoO_3 in the glass. Nevo *et. al* [9] have also proposed a structural model of tellurite glasses in the TeO_2-Fe_2O_3 systems with high concentrations of TeO_2 based on neutron diffraction analysis. According to their model, the basic coordination polyhedron is the tribunal bipyramid TeO_4 connected through bridging oxygen atoms while Fe atoms assume octahedral arrangement to the oxygen atoms. They do not exclude the possibility of the TeO_3 polyhedra formation, even though its contribution to the radial distribution function (RDF) is considered to be small.

The purpose of the present work is to establish what structural changes may be registered by FTIR spectra in short range order as a consequence of adding MoO_3 as a modifier with different concentrations of the glasses system ($TeO_{2(100-x)}$-$MoO_{3(x)}$).

The results of Fourier transform infrared (FTIR) spectrophotometer are believed to help interpreting our results.

2. Experiment

The glasses under study have been prepared by mixing high purity TeO2 and MoO3 in specified contains. By using alumina crucibles, the oxides melted in an electrical furnace held at 800-850°C depending on the contained of MoO_3 for 1 hour and quenched rapidly at 300°C for 1 hour. The prepared samples were examined by x-ray diffraction (XRD) for distinguishing the glassy states. The FTIR absorption spectra of the prepared glasses in KBr matrix were recorded on a SHIMADZU-8300 FTIR spectrophotometer at room temperature. The produced glasses were thoroughly grounded and mixed with equal ratio of KBr. The pellets were clean and uniform. The FTIR absorption spectra of the prepared glasses as a bulk were recorded as shown in figure (1).

3. Result and Discussion

The FTIR spectra of the glasses have been studied together with the spectra for crystalline TeO_2, which are presented in figures (1) and (2). By comparing the present spectra of the glasses with their crystalline constituents [10], it has been found that most of the sharp bands characteristic of the crystalline TeO_2 were disappeared in figures (1) and (2). The bands have broadened and shifted slightly ongoing from the crystalline to the amorphous (glassy) state, while new bands have appeared by the addition of MoO_3 oxide.

Figure (1) shows the FTIR spectra of the glasses as a bulk. It shows a broad band corresponding in the OH stretching (ν_{OH}) at 3143 cm^{-1} for pure TeO_2. This band may be due to presence of the inclusion of water molecules in the pores.

The most diagnostic peaks have been shown in Table (1). Figure (2) shows the FTIR spectra of the glass system with KBr in pellet form. The main infrared band at 625 cm^{-1} which is attributed to symmetrical stretching vibration of Te-O_{ax} bonds in the deformed TeO_4 units. By analogy with the crystalline TeO_2, it may be concluded that the maximum do belong to deformed TeO_4 groups. Dimitrive *et. al* [6] concluded that glasses containing symmetric TeO_4 groups equivalent to maximum at 670 cm^{-1} and shoulder at 635 cm^{-1}, while glass containing deformed trigonal bipyramid for TeO_4 groups corresponded to a shoulder at 670 cm^{-1} (which we could not find in the present study) and maximum at 635 cm^{-1}.

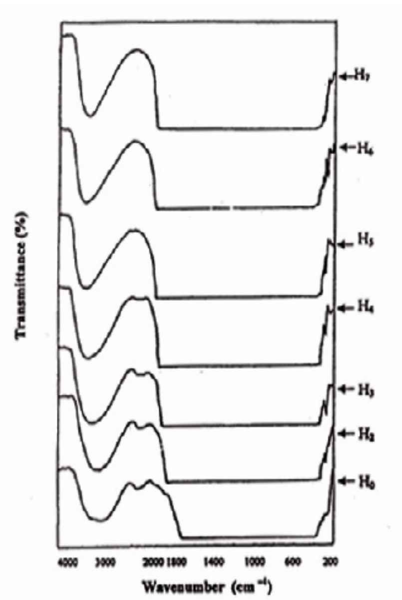

Fig. (1): FTIR spectra of glasses in TeO_2-MoO_3 system as a bulk

Adding MoO_3 to the tellurite glass, the maximum was shifted slightly to higher wavenumber as we increased the modifier content. This is due to changes of coordination state of tellurium atom from TeO_4 through TeO_{3+1} to TeO_3 with bond breakage between tellurium (Te) and axial oxygen (O_{ax}) as we increased the modifier atoms [8] (the notation TeO_{3+1} means that there are three short Te-O bonds and a comparatively longer Te-O bond in the TeO_{3+1} polyhedra) [9].

Table (1) The absorption bands of FTIR spectra for TeO_2-MoO_3 systems [16,18]

Sample No. and Glass System		Infrared absorption band position (cm^{-1})										
	TeO_2 (crystal)[16][18]	-	270	350 [16]	-	-	580	660	771	-	-	-
	TeO_2 (glass) [18]	-	-	340	-	-	-	640	740	-	-	-
Ho	TeO_2 glass	-	268	350	-	-	-	625	-	-	-	3143.8
H2	$(TeO_2)_{90}$ – $MoO_{3\,(10)}$	216	262.3	345	365	-	-	625	-	-	-	3200
H3	$(TeO_2)_{80}$ – $MoO_{3\,(20)}$	214	264	340.6	370	-	-	630	-	840	930	3260
H4	$(TeO_2)_{70}$ – $MoO_{3\,(30)}$	214	264	341	369	-	-	635	-	855	935	3300
H5	$(TeO_2)_{60}$ – $MoO_{3\,(40)}$	214	268.1	339	372	-	-	635	-	864	940	3300
H6	$(TeO_2)_{50}$ – $MoO_{3\,(50)}$	214	264	329	372	-	-	640	-	870	950	3300
H7	$(TeO_2)_{45}$ – $MoO_{3\,(55)}$	214	260	325	372	-	-	648	-	880	960	3300

Actual tellurite glasses are made up of not only one structural unit but the mixture of TeO_4, TeO_{3+1} and or TeO_3 [7,9]. This is due to the local inhomogeneity. The electrons do not transfer from the modifier atom to all the structural units, and consequently two or more states of the structural unit exist in the actual tellurite glasses. Mochida *et. al* [11] found with the aid of IR spectra and according to Yakhkind [12] that the number of TeO_{3+1} group is stimulates modified oxides. New appearance of the maximum at 840 cm^{-1} as the MoO_3 content increases above 20%wt. is an indication of the growing role of complexes in the formation of the network. This maximum shifts to higher wavenumber as the content of modified oxide (MoO_3) increases. The new shoulder appearing at 930 cm^{-1} can be related to the presence of short, isolated Mo=O bond [13].

In tellurite glasses, however, the modifier atoms play one important role, causing the variation of the structural unit itself. It is in contrast with the structural unit of silicate glasses (a SiO_4 tetrahedron which is not affected by modifier atoms) [8]. So, as the MoO_3 content increases all the Te-O-Te bonds will be attacked and the number of Te-O-Mo bridging bonds will increase without a direct attack on the isolated Mo=O bonds [8]. A similar mechanism has been suggested for glasses of the TeO_2-V_2O_5 system in which a bond corresponding to V=0 vibrations is found at 975 cm^{-1} [14]. The maximum at 840 cm^{-1} could be attributed to the stretching vibration modes of equatorial bonds of Mo-O [13].

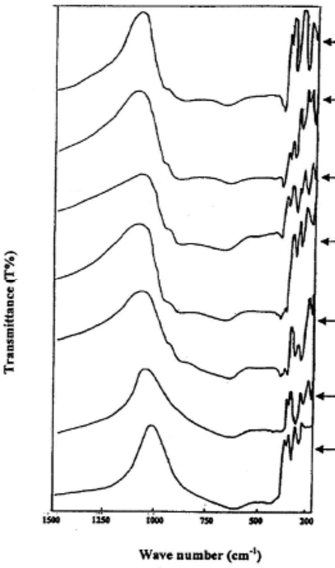

Fig. (2): FTIR spectra of glasses in TeO_2-MoO_3 system with KBr in pellet form

4. Conclusion

New peaks at (389-372) cm^{-1} have been observed by FTIR spectra, their sources have not clearly been identified but Cheromisinov and Zlomanov [15], from their analysis by Raman spectrum of TeO_2 [both crystalline and amorphous], suggested that these peaks are related to various modes of TeO_4 units and are not connected to the formation of TeO_3 pyramids.

We suggest that they may be due to the various modes of Te_{03+1} units. The increase in the intensity of these peaks with the addition of MoO_3 gives a supports to the above suggestion. Two other peaks of 350 cm^{-1} and 268 cm^{-1} have been noticed in all studied TeO_2 glass systems and the maxima at 350 cm^{-1} and 268 cm^{-1} were noticed as well in the crystalline TeO_2 [16]. This means that they all belong to Te-O modes of vibration.

A maximum at about 216-214 cm^{-1}, which appeared by adding MoO_3, may be due to non-bridging oxygen atoms, which is confirmed to be exist in the structure by Nevo *et al.* [9] for TeO_2-Fe_2O_3 glasses. Jong Heo *et al.* [17] suggest the presence of non-bridging oxygen atoms in Li_2O-TeO_2 and Na_2O-TeO_3 systems and this is confirmed by Sekiya *et al.* [7] on alkali tellurite glasses.

References

[1] Stanworth, J.F., *J. Soc. Glass. Tech.*, 36 (1952) 171.

[2] Sarjeant, P.T. and Ray, R., *J. Amer. Soc.*, 50 (1967) 500.

[3] Dimitriv, Y., Marinov, M. and Stoyanov, A., *Acad. Bulg. Sci.*, 21 (1986) 66.

[4] Al-Ani, S.K.J., Hogarth, C.A. and El-Mallawany, R., *J. Mater. Sci.*, 20 (1985) 667.

[5] Congshan, Z., Xiaojuan, L. and Zuyi, Z., *J. Non-Cryst. Solids*, 144 (1992) 89.

[6] Dimitrive, Y., Dimitriov, V. and Arnaudov, M., *J. Mater. Sci.,*18 (1983) 1353.

[7] Sekiya, T., Mochida, M., Ohtsuka, A. and Tonokawa, M., *J. Non-Cryst. Solids*, 144 (1992) 128.

[8] Shigera, S., Yamamoto, K., Hishita, S. and Aizawa, T., *Phys. Rev. B*, 51 (1995) 21.

[9] Nevo, S., Gerassimova, I., Krezhev, K., Syzhimov, B. and Kozhukharov, V. *phys. stat. solidi.* (a), 47 (1978) 743.

[10] Hassan, M.A., Khleif, W.I. and Hogarth, C.A, *J. Mater. Sci.*, 24 (1989) 1607.

[11] Mochida, N., Takashi, K., Nakato, K., Shibusawa, S. and Kuokaishi, Y., Yogyo-Kyokai Shi (online journal in Japanese), 86 (1978) 317.

[12] Yakhklnd, A.K., "Structure and physio-chemical properties of inorganic glasses" (in Russian), Edited by A.G. Vlosov and V.A. Florinska (Khimiya, Linengrad) (1974) 67.

[13] Nakamoto, K., "Infrared and Raman spectra of Inorganic and coordination compound", 4th ed., John-Wiley & Sons (1986) 109.

[14] Kohn, K., Inone, K., Horie, O. and Akimoto, S., *J. Solid State Chem.*, 18 (1976) 27.

[15] Cheremisinov, V.P. and Zlomanov, V.P., *Opt. Spectroscop.*, (Engl. Trans.) 107 (1962) 110.

[16] Khan, M.N., *phys. stat. solidi.* (a), 114 (1989) 285.

[17] Heo, J., Lam, D., George Jr., H., Mendoza, S.E. and Hensley, D., *J. Amer. Ceram. Soc.*, 75 (1992) 277.

[18] El-Mallawany, R.A., *Infrared Phys.*, 29(2-4) (1989) 781.

This article was reviewed at The Department of Physics, Harcourt Butler Technological Institute, Kanpur, INDIA and School of Applied Sciences, University of Technology, Baghdad, IRAQ

The 8th International Conference on Electrical Fuses and their Applications (ICEFA),

Septermber 2007, Clermont-Ferrand, France

Approximate organisational timetable for ICEFA 2007

Jan. 2006	Despatch of the "First Announcement and Call for Papers"
Mar. 2006	Despatch of the "Second Announcement and Call for Papers" (reminder)
Jun. 2006	Deadline for abstracts
Jan. 2007	Deadline for full papers
Apr. 2007	Deadline for advance registration of delegates and hotel booking
Sep. 2007	Conference

ICEFA 2007: Instructions for Abstract Submission

First Author[1], Second Author[2], and Third Author[3]

[1] Affiliation, Phone Number, Fax Number, Address, E-mail Address
[2,3] Affiliation, Address, E-mail Address

Corresponding Preliminary List of Topics.

Please select the topic corresponding to your abstract from the list below.

1	Manufacturing
2	Technology and Design
3	Circuit Protection, Coordination with Electrical Systems and Apparatus, Applications and Semiconductor Protection
4	Hazard and Environmental Aspects
5	Environmental Protection
6	Arcs in Air and Flash Hazards
7	Fundamental Processes
8	Arcing Phenomena
9	Plasma Interaction with Insulators in Fuses
10	Diagnostics
11	Fuse Operation
12	Standards and Testing

Abstract.

Abstracts should describe original work, not previously published, which should clearly indicate the new and significant advances and their importance. Abstracts should be followed by a keywords list as:

Keywords: keyword a, keyword b, keyword c, keyword d, keyword e.

Submitted files should not exceed 1Mb, one page and you are welcome to send a PDF file version or a WORD file version of your article. We suggest you to call it with your name followed by extension (name.pdf or name.doc) and the file should be submitted by e-mail (icefa@univ-bpclermont.fr) or CD-Rom sent by mail to the following address:

W. Bussière
LAEPT CNRS UMR 6069
Phys. Bat. 5 – Univ. Blaise Pascal
24, Avenue des Landais
63177 AUBIERE CEDEX
FRANCE

Iraqi J. of Appl. Phys. , Vol. 2 , No. 1-2 , 2006 , 27-30

Fatin A.J. Al-Moudarris[*]
Sabah M. Juma
Ahmad K. Ahmad

Department of Physics, College of Science, Al-Nahrain University, Baghdad, Iraq,
[*] fatin_almoudarris@yahoo.com

Design of a Multi-Electrode Immersion Lens for Ion-Optical Systems

The present work puts forward an electrostatic optical device for application in an ion-optical system. A design has been achieved computationally for a multi-electrode immersion lens of low relative spherical and chromatic aberration coefficients with the aid of the following suggested expression for the potential field: $U(z)=[(a*z)/(z_2+c)]+b$ where a, b, and c are constants, z is the optical axis, and U(z) is the axial potential distribution. The potential is constant at the boundaries, therefore the electric field is zero, i.e. there is a field-free region outside the lens where the charged particles travel in a straight line. The lens consists of four electrodes where the terminal electrodes are identical in their geometry. The two inner electrodes have the same shape of a thin disc and their central holes are equal. The lens is not symmetrical about the origin but is rotationally symmetric. The paraxial ray equation has been solved using Runge-Kutta method for the zero and infinite modes of operation. The spherical and chromatic aberration coefficients C_s and C_c, respectively have been computed using Simpson's rule. The following results are obtained for C_s and C_c normalized in terms of the focal length f: $(C_s/f)_{min}=1.3$ and $C_c/f=5$ for zero magnification; $(C_s/f)_{min}=14.42$ and $C_c/f=5.73$ for infinite magnification. These results suggest that operating the proposed lens under zero magnification conditions is more favorable. Therefore, the proposed expression for the potential distribution is recommended for representing an electrostatic immersion lens of low relative chromatic aberration coefficient.

Keywords: *Electrostatic lenses, Ion-optical system, Spherical aberration, Chromatic aberration*

Received: 15 March 2005, Revised: 4 May 2006, Accepted: 20 June 2006

1. Introduction

Electrostatic lenses are finding increasing applications in many areas of science and technology particularly in modern ion implantation instruments. Ion implantation is one of the key technologies in the fabrication of dimensionally controlled semiconductor structures. [1,2].

For the last several decades, many efforts have been made to combine a transmission electron microscope (TEM) with ion implanters [3-5]. This system avoids the problems of transferring samples from the ion implanters to the electron microscope [6]. In situ TEM experiments have the specific advantage that defect clusters produced by heavy ion implantation can be directly correlated to the appearance of highly disordered or amorphous zones for a given ion impact, since the same sample area is monitored during the implantation itself [7]. Ions can be accelerated and introduced into TEM column through an electrostatic system of lenses. This paper aims at investigating what can be theoretically achieved when a proposed rotationally symmetric electrostatic immersion lens is operated in an ion-optical system under zero and infinite magnification conditions with low aberration coefficients.

2. Electrostatic Lens Model

It is often desirable to perform a rapid approximate evaluation of lens properties without actually carrying out a detailed analysis. This can be accomplished with the aid of a simple mathematical model for the lens, i.e. an approximation for the axial potential distribution that is reasonably close to the real one and allows a solution in closed form or an approximation in simple terms. The lens models are basically of two types: The potential distribution is either approximated by a single function for the whole lens (analytical models) or it is divided into a series of intervals and the distribution in each interval is approximated by an elementary function (piecewise models) [8].

It is aimed in the present work to find a more simple analytic expression that would describe the axial potential distribution of an accelerating immersion lens with acceptable aberrations. Since the lens is of the accelerating type, hence the ion beam enters the low potential electrode and emerges from the higher potential electrode.

The following expression is suggested to represent the potential distribution along the optical axis of an immersion lens:

$U(z)=[(a\text{x}z)/(z^2+c)]+b$ (1)

where a, b, and c are constants, z is the optical axis, and $U(z)$ is the axial potential distribution. Plots of $U(z)$ as a function of z are shown in Fig. (1) for different values of a. An increase in the value of a will increase the potential at the middle electrodes while the ratio of the potentials between the outer electrodes changes very slightly. The broken line is the first derivative of the potential distribution when a=6V.mm, b=1.9V and c=3mm^2. It should be mentioned that the above values of b and c have been maintained throughout the present work since both put limitations to the beam trajectory and the lens aberrations. For instance values of b less than 1.9V will change the lens into a diverging instead of converging one. Furthermore, this value of c will offer the lowest aberrations possible. Figure (1) shows that the potential is constant at the lens boundaries, so its first derivative is zero; this means that there is a field-free region outside the lens where the charged particles travel in a straight line. The potential applied on the electrodes at object plane is U_0 and that at the image plane is U_i. The different potentials applied on the four electrodes depend on the value of a taken into consideration.

From the values of the axial potential distribution and its first and second derivatives the electrodes profile has been obtained as shown in Fig. (2). The radial and the axial dimensions of the electrodes r and z respectively have been normalized in terms of the total lens length L which has been taken in the present work to be equal to 40mm as shown in Fig. (1) by the axial extension of the field $U(z)$. It is seen that the immersion lens consists of four electrodes. The terminal electrodes are identical in their geometry. The inner electrodes have the same shape of a thin disc and their central holes are equal which allow passage for the ion beam. The four electrodes have rotational symmetry about the optical axis. The two halves of the lens have a mirror image.

3. The Trajectory of Charged Particles

The trajectory of charged particles through an axially symmetric electrostatic lens field, in terms of the axial potential field $U(z)$ and its first and second derivatives $U'(z)$ and $U''(z)$ respectively, is given by the following paraxial ray equation [9]:

$$r''(z)+r'(z)\frac{U'(z)}{2U''(z)}+r(z)\frac{U''(z)}{4U(z)}=0 \qquad (2)$$

where r is the radial displacement of the beam from the optical axis z, and the primes denote a derivative with respect to z.

Figures (3) and (4) represent the trajectories of the charged particles traversing the field of the immersion lens operated under zero and infinite magnification condition respectively. Under zero magnification condition the charged particles enter the lens field parallel to the optical axis. The gradient of the emerging beam increases with the increase of a, keeping b and c in Eq. (1) constants at the values 1.9V and 3mm^2, respectively. Under infinite magnification condition the charged particles emerge from the lens field parallel to the optical axis. The beam crosses the optical axis within the lens field at the values of $a \geq 3$V.mm.

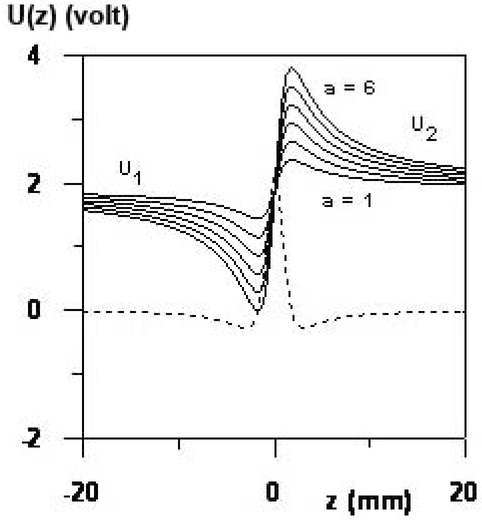

Fig. (1): The axial potential distribution along the optical axis for different values of *a*

4. Spherical and Chromatic Aberration Coefficients

The spherical and chromatic aberration coefficients C_{so} and C_{co} respectively at the object plane have been computed with the aid of the two following formulae [9]:

$$C_{so}=\frac{1}{\sqrt{U_o}\,16r_o'^4}\int_{z_o}^{z_i}\left[\frac{5}{4}\left(\frac{U''}{U}\right)^2+\frac{5}{24}\left(\frac{U'}{U}\right)^4\right. \qquad (3)$$

$$\left.+\frac{14}{3}\left(\frac{U'}{U}\right)^3\frac{r'}{r}-\frac{3}{2}\left(\frac{U'}{U}\right)^2\frac{r'^2}{r^2}\right]\sqrt{U}r^r dz$$

$$C_{co}=\frac{\sqrt{U_o}}{r_o'^2}\int_{z_o}^{z_i}\left[\left(\frac{U'}{U}\right)r'+\frac{1}{4}\left(\frac{U''}{U}\right)r\right]\frac{r}{\sqrt{U}}dz \qquad (4)$$

where U_0 is the potential at the object plane. It should be noted that the corresponding aberration coefficients at the image plane could be expressed in a similar form of equations (3) and (4) when $U_0^{1/2}$ and r'_0 are replaced by $U_i^{1/2}$ and r'_I, respectively. The integration given in the above equations have been executed by means of Simpson’s rule. The aberration coefficients have been normalized in terms of the focal length f, i.e., the values of C_s/f and C_c/f have been investigated as figures of merit, which are dimensionless.

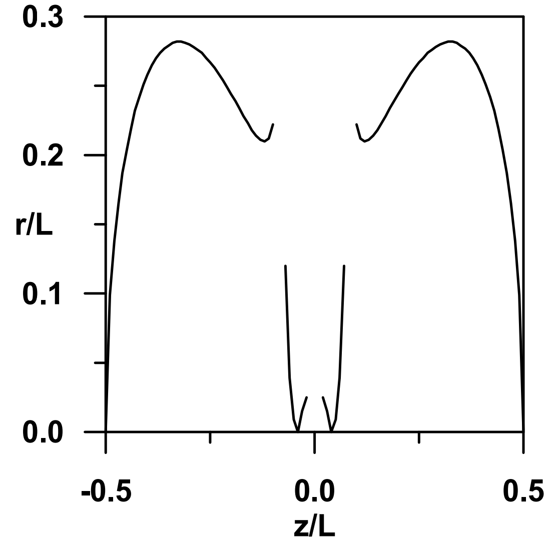

Fig. (2): The electrodes profile of the four-electrode electrostatic immersion lens

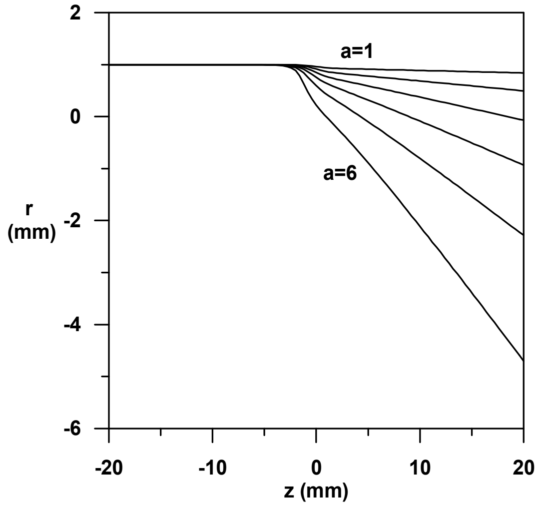

Fig. (3): Trajectory of charged particles traversing the field of the lens operated under zero magnification conditions

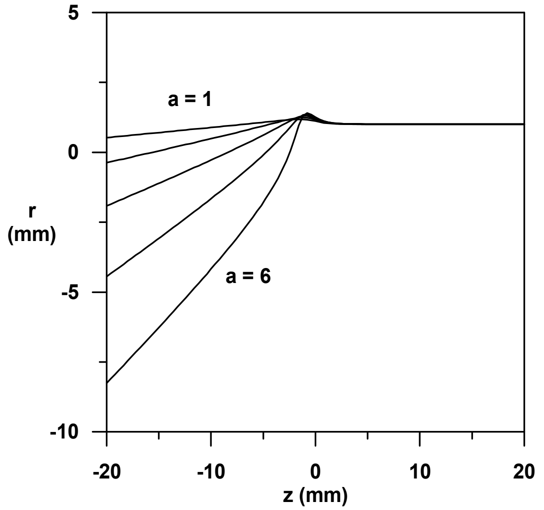

Fig. (4): Trajectory of charged particles traversing the field of the lens operated under infinite magnification conditions

Figure (5) shows the relative image-side spherical and chromatic aberration coefficients C_s/f and C_c/f, respectively, as a function of a for the electrostatic immersion lens operated under zero magnification conditions. It is seen that as a increases, C_s/f decreases towards a minimum value; $(C_s/f)_{\min}=1.3$ at $a=6$V.mm and voltage ratio $U_i/U_0=1.37$. This minimum value is electron-optically acceptable. At this value of a the corresponding relative chromatic aberration $C_c/f=5.0$, which is relatively high from the electron-optical point of view. The figure shows that C_c/f increases with increasing a.

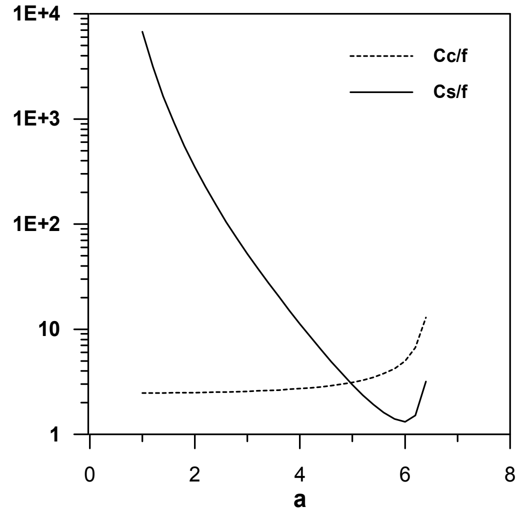

Fig. (5): The relative image-side spherical and chromatic aberration coefficients *Cs/f* and *Cc/f*, respectively as a function of a for an immersion lens operated under zero magnification conditions

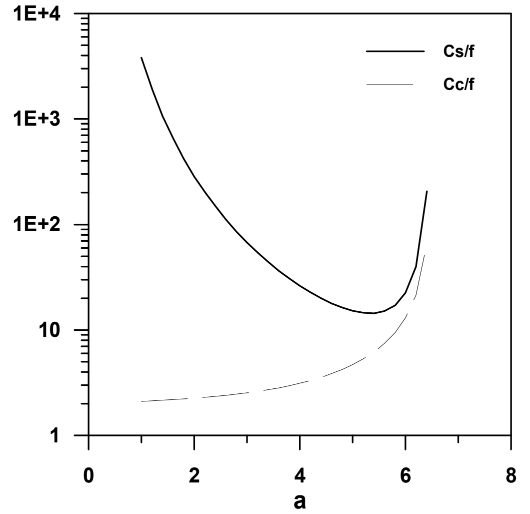

Fig. (6): The relative spherical and chromatic aberration coefficients *Cs/f* and *Cc/f*, respectively as a function of a for an immersion lens operated under infinite magnification conditions

The plots of C_s/f and C_c/f as a function of a for the electrostatic immersion lens operated under infinite magnification condition are shown in Fig. (6). In general the behavior of C_s/f and C_c/f is similar to that shown in Fig. (5). However, the values of the relative aberration coefficients under zero magnification are less than those under infinite magnification, which are $(C_s/f)_{\min}=14.42$ and $C_c/f=5.73$ at $a=5.3$V.mm and $U_i/U_0=1.32$.

It is seen that under both magnification conditions the values of C_c/f are comparable when C_s/f is minimum. Thus, so far as C_s/f is concerned it is favorable to operate this lens under zero magnification condition, i.e., the lens would form a focused ion beam on the image side when a beam parallel to the optical axis enters the lens. However, if one is interested in having both relative aberrations as low as possible, then it is possible to reach a compromise. For instance, at $a=5$V.mm, Fig. (5) shows that C_s/f and C_c/f are equal to 3; a value usually acceptable in practice.

4. Conclusions

It appears that the proposed analytic function of the axial potential field for an immersion lens offers considerable advantages with regard to the relative spherical aberration coefficient, particularly when the lens is operated under zero magnification conditions. This mode of operation is suitable for using the lens as a focusing unit in an ion-optical system. The operation of the proposed immersion lens is limited by its relative chromatic aberration in both zero and infinite magnification conditions. However, this lens may be introduced in various systems such as TEM and ion implanters to focus the beam on the target.

References

[1] Priolo, F., Privitera, V., Coffa, S. and Libertion, S., *Mater. Res. Soc. Symp. Proc.*, 438 (1997) 7401.

[2] Mayers, S.M., Petersen, G.A., Headly, T.J., Aselage, J.R. and Seager, C.H., *Nucl. Instrum. Meth. Phys. Res.*, B127/128 (1997) 291.

[3] Ishikawa, N. and Furuya, K., *Ultramicroscopy*, 56 (1994) 211.

[4] Allen, C.W., *Ultramicroscopy*, 56 (1994) 200.

[5] Takeyama, T., Ohnuki, S. and Takahashi, H., *J. Nucl. Mater.*, 133/134 (1985) 571.

[6] Ruault, M., Chaumont, J. and Bernas, H., *Nucl. Instrum. Meth. Phys. Res.*, 209/210 (1983) 351.

[7] Ruault, M., Lerme, M., Jouffrey, B. and Chaumont, J., *J. Phys E: Sci. Instrum.*, 11 (1978) 1125.

[8] Szilagyi, M., "Electron and Ion Optics", Plenum Press (New York) (1988).

[9] Scheinifein, M. and Galantai, A., *Optik*, 74 (1986) 154.

This article was reviewed at Woods Hole Oceanographic Institution, Massachusetts, U.S.A and School of Applied Sciences, University of Technology, Baghdad, IRAQ

Iraqi J. of Appl. Phys. , Vol. 2 , No. 1-2 , 2006 , 31-36

Alaa B. Kadhem
Ehsan M. Raheem

Ministry of Science and Technology, Applied Physics Research Center, Baghdad, IRAQ

Calculation of Charge Density Distribution of (2s-1d) Shell-Model Nuclei Using the Occupation Numbers of States

The charge density distribution (CDD) of ^{24}Mg, ^{28}Si, ^{30}Si, ^{32}S and ^{34}S nuclei have been calculated using the wave functions of the harmonic oscillator on the assumption that the occupation numbers of the states in real nuclei differ from the predictions of the simple shell model. The difference of the CDD of (^{28}Si-^{30}Si) and (^{32}S-^{34}S) isotopes have been calculated to clarify the influence of the additional neutrons on the CDD. The elastic electron scattering form factors of the considered nuclei have been calculated using the ground state charge density distributions.

Introducing an additional parameter (α) that reflects the difference of the occupation numbers of states between the real states of the nuclei and the simple shell model predictions, leads to a very good agreement between the calculated and experimental results of the CDD and form factors. This leads to the conclusion that proposing (α) as an additional parameter is a real one.

Keywords: *Electrostatic lenses, Ion-optical system, Spherical aberration, Chromatic aberration*

Received: 26 March 2006, Revised: 12 June 2006, Accepted: 25 June 2006

1. Introduction

The charge density distribution (CDD) is a fundamental characteristic of the nucleus in its ground states, and elastic electron scattering is a unique method of determination of this quantity. Here, the larger the momentum-transfer to the nucleus the more accurate is the CDD extracted from such experiment.

Various theoretical methods are used for calculations of the CDD, among them the Hartree-Fock (HF) method with Skyrme effective interaction [1,2], the theory of finite Fermi systems (TFFS) [3,4] and the single particle potential (SPP) method [5]. In the Hartree-Fock in addition to the Skyrme forces SI–SVI, the multiparametric forces Ska, Skb, ST, SM and SM* with up to ten parameters [6] are used. In the HF method the energy dependence of the effective interaction is not taken into account. Taking into account retardation effects in the TFFS improves the description of entire set of data in comparison with the HF method with effective forces [4]. However, the TFFS describes properties of medium and heavy nuclei and is inapplicable to light nuclei. In the SPP method [5] instead of the wave function of the nucleus one introduced the single particle density matrix n^1 containing complete information on the single particle properties of the nucleus. The method is close to the HF method, but here fractional filling numbers of the state n_α, which are determined from experiment, are introduced.

2. The Theory

2.1 Charge Density Distributions

The charge density distribution CDD of the shell nuclei can be evaluated by means of the wave functions of a harmonic oscillator, since [7]:

$$\rho(r)=\frac{1}{4\pi}\sum_{nl}(2j+1)R_{nl}^2(r) \qquad (1)$$

where $R_{nl}(r)$ is the radial part of the harmonic oscillator wave function, which is given by [8]:

$$R_{nl}^2(r)=[(\pi^{1/2}b^3).\{(2l+1)!!\}^2.(n-1)!]^{-1}.2^{l-n+3}.(2l+2n-1)!!.(\frac{r}{b})^{2l}$$
$$*\sum_{k=0}^{n-1}[(-1)^k.\{(n-1-k)!k!(2k+2l+1)!!\}^{-1}.2^k.(n-1)!(2l+1)!!(\frac{r}{b})^{2k}]^2*\exp(-r^2/b^2) \qquad (2)$$

Putting Eq. (2) into Eq. (1), in the simple shell model, the CDD for 2s-1d shell nuclei are:

$$\rho(r) = \frac{1}{\pi^{3/2} b^3}\{5 + (\frac{4}{15}Z - \frac{4}{3})(\frac{r}{b})^4\}.\exp(-r^2/b^2) \quad (3)$$

where Z is the charge of the nucleus and b is the oscillator parameter.

Eq. (3) gives the CDD of 2s-1d shell nuclei on the bases of the simple shell model.

The mean square radii (MSR) of the considered nuclei are obtained according to the following equation [9]:

$$\langle r^2 \rangle = \frac{4\pi}{Z}\int_0^\infty \rho(r) r^4 \, dr \quad (4)$$

The normalization of the CDD is given by [10]:

$$Z = 4\pi \int_0^\infty \rho(r) r^2 \, dr \quad (5)$$

Substituting the form of the CDD of eq.(3) into eq.(4), we obtain the (MSR) of 2s-1d shell nuclei:

$$\langle r^2 \rangle = \frac{b^2}{2}[7 - \frac{20}{Z}] \quad (6)$$

In the present work, the CDD of the 2s-1d shell nuclei are calculated by means of the harmonic oscillator wave functions on assumption that filling numbers of the states in real nuclei differ from the predictions of the simplest shell-model. These numbers can be determined from the comparison between the calculated and the experimental charge density distribution. Therefore, with this assumption, the CDD for 2s-1d shell nuclei are:

$$\rho(r) = \frac{1}{\pi^{3/2} b^3}\{5 - \frac{3}{2}\alpha + 2\alpha(\frac{r}{b})^2 + (\frac{4}{15}Z - \frac{4}{3} - \frac{2}{5}\alpha_1 - \frac{2}{3}(\alpha - \alpha_1)\,)(\frac{r}{b})^4 + \frac{8}{105}(\alpha - \alpha_1)(\frac{r}{b})^6\}.\exp(-r^2/b^2) \quad (7)$$

where the parameter α which is equal to $\alpha_1+\alpha_2$ characterizes the deviation of filling numbers from the predictions of the shell-model. The CDD of Eq. (7) is obtained on the assumption that there is a core of filled 1s and 1p shells, and the proton numbers in 2s,1d and 1f shells are equal to, respectively, $2\text{-}\alpha$, $Z\text{-}10+\alpha$ and α_2 (in real nucleus) instead of 2, Z-10 and zero (as in the simple shell model of Eq. (3)), where the parameters α, α_1 and α_2 represent the deviation of the shell charges of 2s, 1d and 1f from the prediction of the simple shell model. The parameter α is determined from the central CDD, ρ(r=0), of Eq. (7), i.e.,

$$\rho(0) = \frac{1}{\pi^{3/2} b^3}(5 - \frac{3}{2}\alpha) \quad (8)$$

Since the values of $\rho(0)$ are known, i.e., they can be taken from experiments. The harmonic oscillator size parameter b are obtained by introducing the experimental MSR of considered nuclei into Eq. (6). The parameters α_1 and α_2 are determined by:

$$\alpha_1 = \frac{2}{3}(5 - \pi^{3/2} b^3 \rho(0)) - \frac{Z}{b^2}\langle r^2 \rangle - 10 + \frac{7}{2}Z \quad (9)$$

$$\alpha_2 = \frac{Z}{b^2}\langle r^2 \rangle + 10 - \frac{7}{2}Z \quad (10)$$

2.2 Elastic Electron Scattering Form Factors

The elastic electron scattering form factors from spin zero nuclei can be determined by the ground-state charge density distributions. In Plane Wave Born Approximation (PWBA), the incident and scattered electron waves are considered as plane waves and although this seems to be somewhat reasonable, an accurate testing of the experimental cross section values and other observable leads to the realization that using PWBA provides mainly qualitative description even for light nuclei [11,12]. Therefore, in PWBA and if the CDD is real and spherical symmetric, the form factor is simply the Fourier transform of the CDD and it is real and spherical symmetric, and vice versa [13,14]. Thus:

$$F(q) = \frac{4\pi}{Z}\int_0^\infty \rho(r) j_0(qr).r^2 \, dr \quad (11)$$

where $j_0(qr) = \sin(qr)/dr$ is the zeroth-order spherical Bessel function and q is the momentum transfer from the incident electron to the target nucleus. Eq. (11) may be expressed as:

$$F(q) = \frac{4\pi}{qZ}\int_0^\infty \rho(r)\sin(qr) r \, dr \quad (12)$$

The form factors of the 2s-1d shell nuclei in the simple shell model (i.e. α=0) can be obtained by introducing the form of the CDD of Eq. (3) into Eq. (12), i.e.,

$$F(q) = \frac{1}{Z}\{Z + \frac{1}{3}(5 - Z)q^2 b^2 + \frac{1}{12}(\frac{Z}{5} - 1)q^4 b^4\}.\exp(-\frac{q^2 b^2}{4}) \quad (13)$$

Similarly, the form factors of the above nuclei according to our assumption (i.e., $\alpha \neq 0$) can be obtained by introducing the CDD of Eq. (7) into Eq. (12), i.e.,

$$F(q) = \frac{1}{Z}\{Z + (\frac{5}{3} - \frac{Z}{3} - \frac{1}{6}\alpha + \frac{1}{6}\alpha_1)q^2 b^2 + (\frac{Z}{60} - \frac{1}{12} + \frac{1}{120}\alpha - \frac{1}{30}\alpha_1)q^4 b^4 - [\frac{(\alpha - \alpha_1)}{840}]q^6 b^6\}.\exp(-\frac{q^2 b^2}{4}) \quad (14)$$

3. Results and Discussion

The calculated CDD of ^{28}Si, ^{30}Si, ^{32}S and ^{34}S nuclei have been compared with the fitted to the experimental data of Model-Independent (MI) CDD [9],while the calculated CDD of ^{24}Mg nucleus has been compared with the fitted to the experimental data of tow Parameter Fermi model (2PF) CDD [15].

In the figures (1) to (5), we present the dependence of the CDD on r for ^{24}Mg, ^{28}Si, ^{30}Si, ^{32}S and ^{34}S nuclei. The squares are the fitted to the experimental CDD, the dashed curves are the calculated CDD with $\alpha \neq 0$ for the above nuclei.

For all considered nuclei that are under investigation, the experimental values of the root mean square charge radii, the central CDD at $r=0$, the calculated values of the size parameter b, the calculated parameters α, α_1 and α_2 of the 2s-1d shell nuclei are presented in table (1). The occupation numbers of 2s, 1d and 1f orbits of 2s-1d shell nuclei are presented in table (2).

Table (1) Parameters of the CDD of 2s-1d shell nuclei

Nucleus	Model	$\langle r^2 \rangle^{1/2}$ fm exp.[9]	$\rho(0)$ $e.fm^{-3}$ exp.[9]	Z	$b\, fm$	α	α_1	α_2
^{24}Mg	2PF	3.03	0.0817	12	1.8554	1.39499	1.39193	3.053x10^{-3}
^{28}Si	MI	3.078	0.0847	14	1.8441	1.36030	1.35745	2.851x10^{-3}
^{30}Si	MI	3.148	0.0763	14	1.8861	1.43175	1.43144	3.078x10^{-3}
^{32}S	MI	3.244	0.090	16	1.9132	0.99223	0.99191	3.255x10^{-4}
^{34}S	MI	3.277	0.0871	16	1.9326	0.99804	0.99476	3.288x10^{-3}

Table (2) Proton occupation numbers of states

Nucleus	Occupation Numbers of 2s	Occupation Numbers of 1d	Occupation Numbers of 1f
^{24}Mg	0.60501	3.39193	3.053x10^{-3}
^{28}Si	0.63970	5.35745	2.851x10^{-3}
^{30}Si	0.56825	5.43144	3.078x10^{-4}
^{32}S	1.00776	6.99191	3.255x10^{-4}
^{34}S	1.00195	6.99476	3.288x10^{-3}

It is evident from figures (1) to (5) of the CDD that the calculated densities with $\alpha=0$ (dashed curves) are in poor agreement with the fitted data, especially for small r. Introducing the parameter α in our calculations, leads to a good agreement, as shown by the solid curve in these figures.

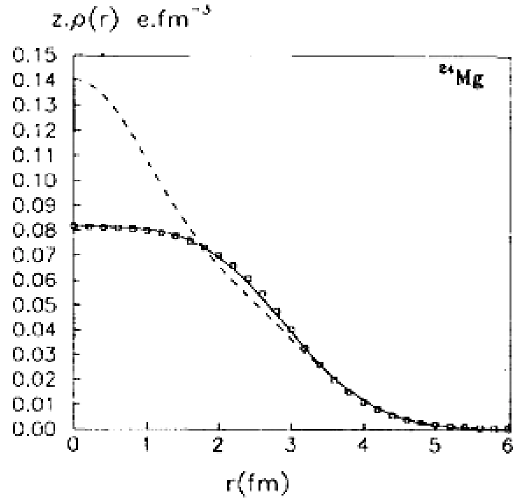

Fig. (1): Dependence of the CDD of ^{24}Mg nucleus on r. the dashed and the solid curves are the calculated CDD of Eq. (7) when $\alpha=0$ and $\alpha\neq0$, respectively. The squares are the fitted to the experimental data of Two Parameter Fermi Model CDD [15] with the parameters c=2.98 f_m and z=0.551 f_m

Inspection of the CDD of the ^{30}Si and ^{34}S nuclei which are shown in figures (3) and (5), indicate that the additional neutrons to the ^{28}Si and ^{32}S nuclei, lead to change slightly the distribution of the protons in the shells because of the nuclear interactions between these additional neutrons and the protons. This interactions leads to some decrease in the CDD especially at the central regions of these nuclei. By the additional neutrons to these nuclei, the charges are removed from the interior and from the tail of the distributions and transferred into the surface regions.

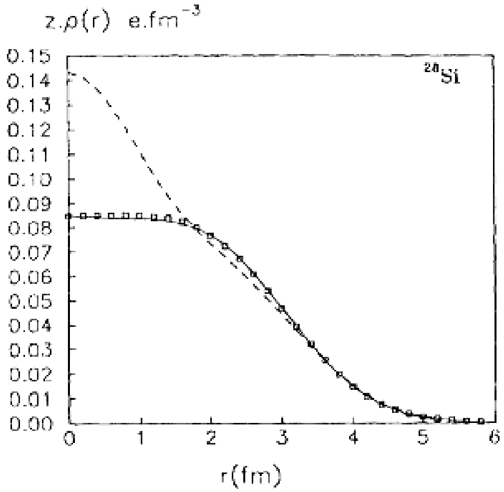

Fig. (2): Dependence of the CDD of ^{28}Si nucleus on r. the dashed and the solid curves are the calculated CDD of Eq. (7) when $\alpha=0$ and $\alpha\neq0$, respectively. The squares are the fitted to the experimental data of Model Independent CDD [9]

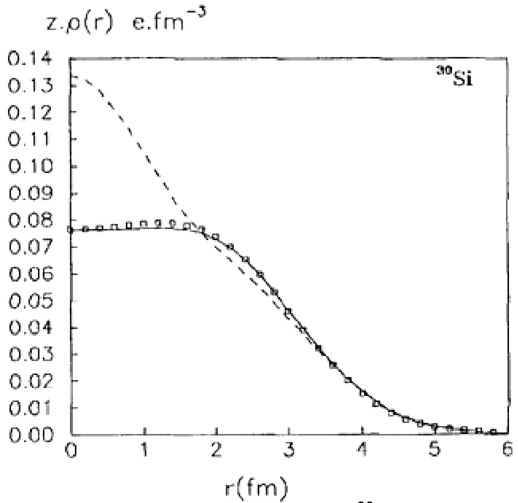

Fig. (3): Same as in Fig. (2) but for ^{30}Si nucleus

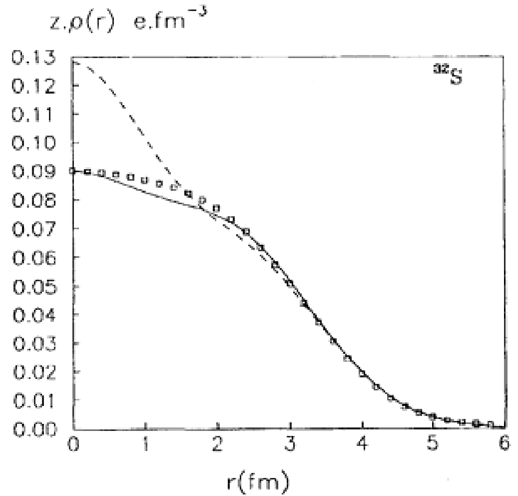

Fig. (4): Same as in Fig. (3) but for ^{32}S nucleus

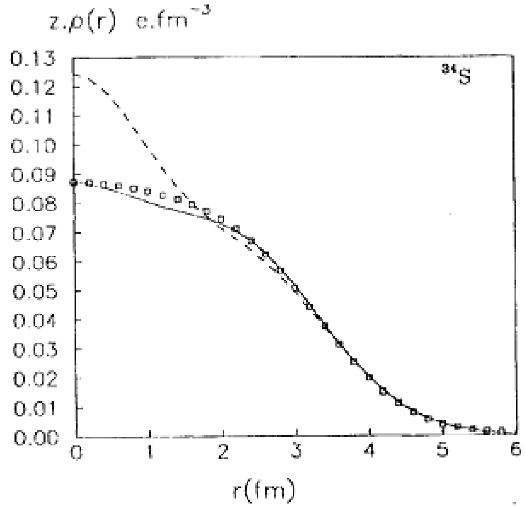

Fig. (5): Same as in Fig. (2) but for ^{34}S nucleus

The difference of the CDD of (^{30}Si-^{28}Si) and (^{34}S-^{32}S) isotopes $\Delta\rho(r)$ are calculated to clarify the influence of the additional neutrons on the CDD as shown in the figures (6) and (7), respectively. The squares are the differences of fitted CDD and the solid curves are the calculated difference of the CDD with $\alpha\neq 0$.

The elastic electron scattering form factors from the considered nuclei are calculated and compared with the experimental data as a function of the momentum-transfer q as shown in the figures (8) to (12), where the circles are the experimental results, squares are the fitted to the experimental data and the solid curves are the calculated results.

The from factors of ^{24}Mg nucleus are presented in figure (8). The experimental data [14] are well described by the calculated data up to $q\approx 3\ fm^{-1}$ as shown by the solid curve. Figures (9) and (10) show the form factors of ^{28}Si and ^{30}Si nuclei, respectively. There is good agreement between the calculated and the experimental data [14] for all momentum transfer values of ^{28}Si nucleus. For ^{30}Si nucleus, the experimental data [16] (circles) are very good described by the calculated data, and the fitted to the experimental data [9] (squares) are described in the region $q\leq 1.45fm^{-1}$, the second diffraction minimum in the fitted data is also described by the calculated data. The form factors of ^{32}S and ^{34}S are displayed in figures (11) and (12), respectively. The experimental data [16] of ^{32}S nucleus and the fitted data [9] of ^{34}S nucleus are very well explained by our calculated form factors. The calculated form factors slightly dispredicts these data at high q values, and it may be attributed to the necessity of introducing the occupation numbers to the shell 2p.

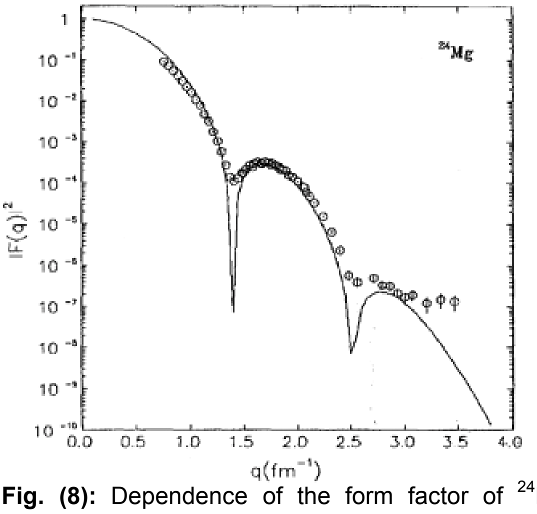

Fig. (8): Dependence of the form factor of ^{24}Mg nucleus on the momentum transfer *q*. The solid curve is the calculated form factor of Eq. (14) with $\alpha\neq 0$. The circles are the experimental data [14]

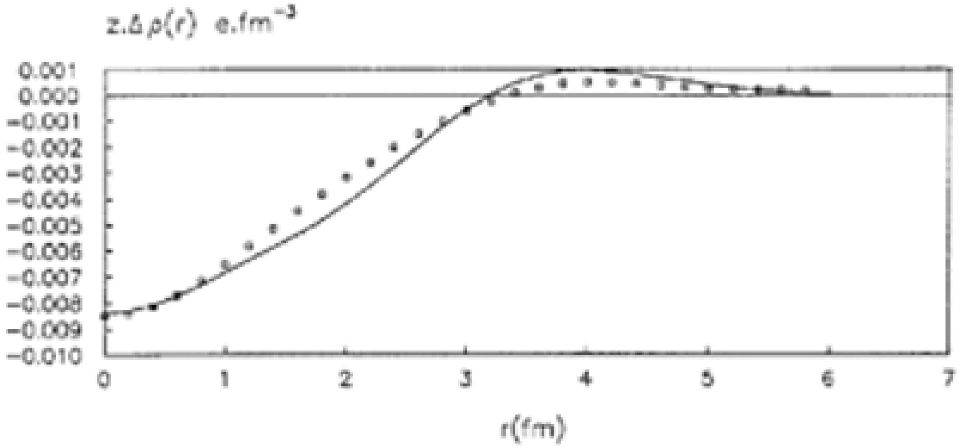

Fig. (6) Dependence of the difference of the CDD of (^{30}Si-^{28}Si) isotopes $Z.\Delta\rho(r)$ on r. The squares are the Model-Independent difference of the CDD. The solid curve is the calculated difference of CDD with $\alpha \neq 0$.

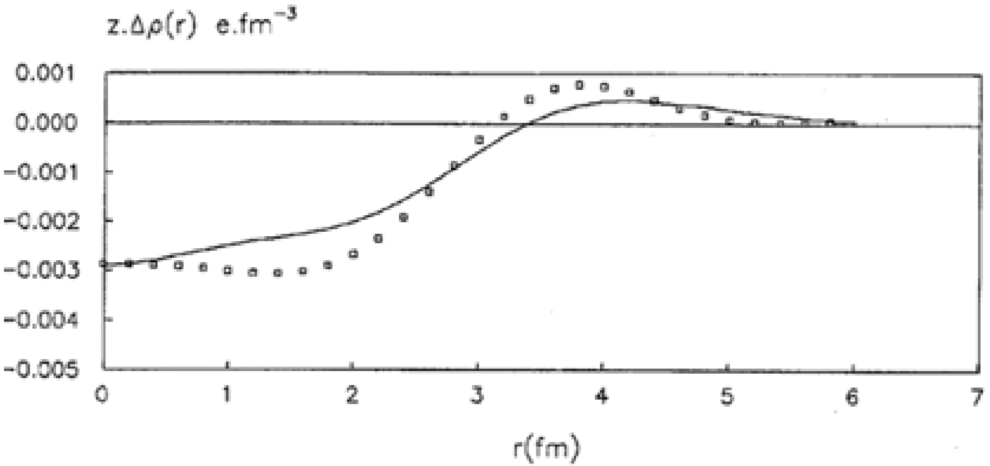

Fig. (7) The same as in Fig. (6) but for (^{34}S-^{32}S) isotopes

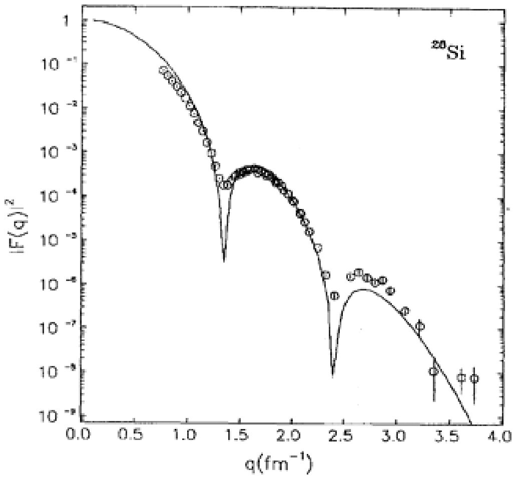

Fig. (9): Same as in Fig. (10) but for ^{28}Si nucleus

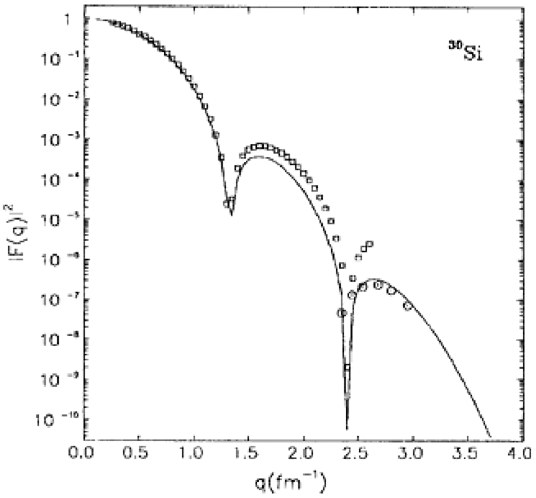

Fig. (10): Same as in Fig. (8) but for ^{30}Si. The circles are the experimental data [16], and the squares are the fitted to the experimental data [9]

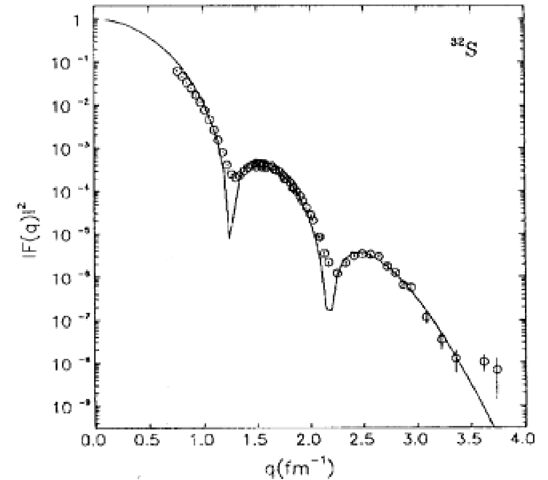

Fig. (11): Same as in Fig. (10) but for ^{32}S nucleus

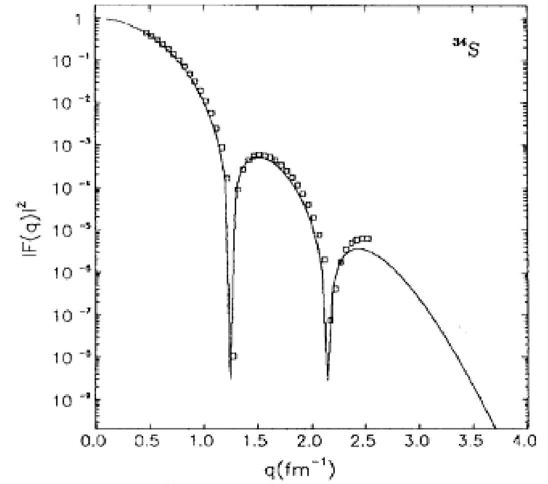

Fig. (12): Same as in Fig. (8) but for ^{34}S. The circles are the experimental data [16], and the squares are the fitted to the experimental data [9]

4. Conclusions

The charge density distribution (CDD) of ^{24}Mg, ^{28}Si, ^{30}Si, ^{32}S and ^{34}S nuclei have been calculated using the wave functions of the harmonic oscillator on the assumption that the occupation numbers of the states in real nuclei differ from the predictions of the simple shell model. The difference of the CDD of (^{28}Si-^{30}Si) and (^{32}S-^{34}S) isotopes have been calculated to clarify the influence of the additional neutrons on the CDD. The elastic electron scattering form factors of the considered nuclei have been calculated using the ground state charge density distributions.

Introducing an additional parameter (α) that reflects the difference of the occupation numbers of states between the real states of the nuclei and the simple shell model predictions, very good agreement between the calculated and experimental results of the CDD and form factors was observed. This leads to the conclusion that proposing (α) as an additional parameter is a real one.

References

[1] Vautherin, D. and Brink, D., *Phys. Rev.* C5 (1972) 626.

[2] Barts, B.I., Bolotin, Yu.L., Inopin, E.V. and Gonchar, V.Yu., "Hartree Fock Method in Nuclear Theory" (in Russian), Kiev, Naukova, Dumka (1982).

[3] Khodel, V.A. and Saperstein, E.E., *Phys. Rep.* 92 (1982) 183.

[4] Saperstein, E.E. and Khodel, V.A., *Sov. J. Nucl. Phys.* 38 (1983) 507.

[5] Antonov, A.N., Hodgson, P.E. and Petkov, I.Zh., "Nucleon Momentum and Density Distribution in Nuclei", Clarendon Press (Oxford) (1988).

[6] Fridrich, J. and Reinhard, P.G., *Phys. Rev.* C33 (1986) 355.

[7] Gul'karov, I.S. and Pinkus, L.D., *Sov. J. Nucl. Phys.* 44 (1986) 210.

[8] Brussard, P.J. and Glaudemans, P.W., "Shell-Model Application in Nuclear Spectroscopy", North-Holland (Amsterdam) (1977).

[9] Atomic Data and Nuclear Data Tables, 36(3), May 1987.

[10] Irvine, J.M., "Nuclear Structure Theory", Pergamon Press (Oxford) (1972).

[11] Lapikas, L., Dieperink, A.E.L. and Box, G., *Nucl. Phys.* A203 (1973) 609.

[12] Chertok, B.T., *Phys. Rev.* 187 (1969) 1340.

[13] Sick, J. and McCarthy, J.S., *Nucl. Phys.* A150 (1970) 631.

[14] Li, G.C., Yearian, M.R. and Sick, I., *Phys. Rev.* C9 (1974) 1861.

[15] Lees, E.W., Curran, C.S., Drake, T.E., Gillespie, W.A., Johanston, A. and Singhal, R.P., *J. Phys.*, G2 (1976) 105.

[16] Wesseling, J. *et al.*, *Phys. Rev.*, C55 (1997) 2773.

This article was reviewed at The Department of Electromagnetism, Faculty of Physics, University of Compostela, SPAIN and School of Applied Sciences, University of Technology, Baghdad, IRAQ

NEW

These title are available on order at very competitive prices.
Order your title now
Contact us … NOW

Sirb Zajil
For Express Mail L.L.C

- THE THEORY OF MAGNETISM MADE SIMPLE: An Introduction to Physical Concepts and to Some Useful Mathematical Methods
  D C Mattis
  (Utah University, USA)
- PRINCIPLES OF QUANTUM COMPUTATION AND INFORMATION Volume I: Basic Concepts
  Giuliano Benenti,
  Giulio Casati &
  Giuliano Strini
  (Universite di Milano, Italy)
- INTRODUCTION TO NUCLEAR AND PARTICLE PHYSICS (Second Edition)
  A Das & T Ferbel
  (University of Rochester, USA)
- HANDBOOK OF ACCELERATOR PHYSICS AND ENGINEERING (3rd Printing)
  Alexander Wu Chao
  (Stanford Linear Accelerator Center) &
  Maury Tigner
  (Cornell University)
- IRON DOMINATED ELECTROMAGNETS - Design, Fabrication, Assembly and Measurements
  Jack T Tanabe
  (Stanford Linear Accelerator Center, USA)
- ACCELERATOR PHYSICS (Second Edition)
  S Y Lee
  (Indiana University, USA)
- PHYSICS OF INTENSE CHARGED PARTICLE BEAMS IN HIGH ENERGY ACCELERATORS
  Ronald C Davidson & Hong Qin
  (Plasma Physics Laboratory and Department of Astrophysical Sciences Princeton University)
- ELECTRODYNAMICS: AN INTRODUCTION INCLUDING QUANTUM EFFECTS
  Harald J W Müller-Kirsten
  (University of Kaiserslautern, Germany)
- THE PHYSICS OF SOLAR CELLS
  Jenny Nelson
  (Imperial College, UK)
- PRINCIPLES OF RADIATION INTERACTION IN MATTER AND DETECTION
  Claude Leroy
  (Université de Montréal, Montréal, Canada)
- ROUGH SURFACES (Second Edition)
  Tom R Thomas
  (Chalmers University of Technology, Sweden)
- AN INTRODUCTION TO ASTROPHYSICAL FLUID DYNAMICS
  Michael J Thompson
  (University of Sheffield, UK)
- ASTRONOMICAL SPECTROSCOPY: An Introduction to the Atomic and Molecular Physics of Astronomical Spectra
  Jonathan Tennyson
  (University College London, UK)
- SPACE SCIENCE
  Louise K Harra & Keith O Mason
  (University College London, UK)
- DYNAMICS OF PARTICLES AND THE ELECTROMAGNETIC FIELD
  Slobodan Danko Bosanac
  (Rudjer Boskovic Institute, Croatia)
- PATH INTEGRALS IN QUANTUM MECHANICS, STATISTICS, POLYMER PHYSICS, AND FINANCIAL MARKETS (4th Edition)
  Hagen Kleinert
  (Freie Universität Berlin, Germany)
- INTRODUCTION TO CONDENSED MATTER PHYSICS “Volume 1”
  Feng Duan & Jin Guojun
  (Nanjing University, China)
- SHOCK WAVES: Measuring the Dynamic Response of Materials
  William M Isbell
  (ATA Associates, USA)
- ELEMENTARY ELECTRONIC STRUCTURE (Revised Edition)
  Walter A Harrison
  (Stanford University, USA)
- FIELD THEORY, THE RENORMALIZATION GROUP, AND CRITICAL PHENOMENA
  (3rd Edition)
  Daniel J Amit
  (Università di Roma, "La Sapienza", Italy) &
  Victor Martin-Mayor
  (Universidad Complutense de Madrid, Spain)
- LATTICE GAUGE THEORIES: An Introduction (Third Edition)
  Heinz J Rothe
  (Universität Heidelberg, Germany)
- SUPERSYMMETRY IN QUANTUM MECHANICS
  Fred Cooper
  (Los Alamos National Laboratory),
  Avinash Khare &
  Uday Sukhatme
  (University of Illinois, Chicago)

- **SCATTERING AND DIFFRACTION IN PHYSICAL OPTICS (2nd Edition)**
  Manuel Nieto-Vesperinas
  (Madrid Institute of Materials Science, Spain)

- **MODERN FOUNDATIONS OF QUANTUM OPTICS**
  Vlatko Vedral (University of Leeds, UK)

- **NEAR-FIELD MICROSCOPY AND NEAR-FIELD OPTICS**
  Daniel Courjon
  (Université de Franche-Comté, France)

- **SHORT PULSE LASER INTERACTIONS WITH MATTER: An Introduction**
  Paul Gibbon (Research Centre Jülich, Germany)

- **PRINCIPLES OF FUSION ENERGY: An Introduction to Fusion Energy for Students of Science and Engineering**
  A A Harms, D R Kingdon
  (McMaster University, Canada)

- **BASIC SPACE PLASMA PHYSICS**
  Wolfgang Baumjohann & Rudolf A Treumann
  (Max-Planck-Institut für Extraterrestrische Physik)

- **ADVANCED SPACE PLASMA PHYSICS**
  R A Treumann & W Baumjohann
  (Max-Planck-Institute für Extraterrestrische Physik)

- **PHYSICS OF NONNEUTRAL PLASMAS**
  Ronald C Davidson (Princeton University)

- **PHYSICS OF INTENSE CHARGED PARTICLE BEAMS IN HIGH ENERGY ACCELERATORS**
  Ronald C Davidson & Hong Qin
  (Plasma Physics Laboratory and Department of Astrophysical Sciences Princeton University)

- **PROBLEMS AND SOLUTIONS IN QUANTUM COMPUTING AND QUANTUM INFORMATION**
  Willi-Hans Steeb & Yorick Hardy
  (Rand Afrikaans University, South Africa)

- **QUANTUM THEORY OF THE OPTICAL AND ELECTRONIC PROPERTIES OF SEMICONDUCTORS (Fourth Edition)**

  Hartmut Haug (Universität Frankfurt, Germany) & Stephan W Koch (Philipps-Universität Marburg, Germany)

- **RELATIVISTIC QUANTUM MECHANICS AND INTRODUCTION TO QUANTUM FIELD THEORY**
  Anton Z Capri (University of Alberta, Canada)

- **QUANTUM FIELD THEORY WITH APPLICATION TO QUANTUM NONLINEAR OPTICS**
  Anatoliy K Prykarpatsky
  (National Academy of Sciences, Ukraine)

- **ELEMENTARY QUANTUM MECHANICS**
  (Expanded Edition)
  Peter Fong (Emory University, USA)

- **EQUILIBRIUM STATISTICAL PHYSICS**
  (3rd Edition)
  Michael Plischke (Simon Fraser University, Canada) & Birger Bergersen (University of British Columbia, Canada)

- **COMPLEXITY AND CRITICALITY**
  Kim Christensen & Nicholas R Moloney
  (Imperial College London, UK)

- **GLASSY MATERIALS AND DISORDERED SOLIDS: An Introduction to Their Statistical Mechanics**
  Kurt Binder (Institut für Physik, Mainz, Germany) & Walter Kob (Laboratoire des Colloïdes, Verres et Nanomatériaux, Montpellier, France)

- **STATISTICAL THERMODYNAMICS AND STOCHASTIC THEORY OF NONEQUILIBRIUM SYSTEMS**
  Werner Ebeling & Igor M Sokolov
  (Humboldt-Universität, Germany)

- **STATISTICAL PHYSICS: Statics, Dynamics and Renormalization**
  Leo P Kadanoff (University of Chicago)

Contact us :

sirb ZAJIL for express mail services

Tel.: +964 1 7175483, IRAQNA: +964 7903221271, ASIACELL: +964 7702523071
www.zajiliraq.com, info@zajiliraq.com, zajil_iraq@yahoo.com

IRAQI JOURNAL OF APPLIED PHYSICS

" INSTRUCTIONS TO AUTHORS "

A new Iraqi specialized quarterly periodical dedicated to publishing original papers and letters in:

Applied & Nonlinear Optics
Applied Mechanics & Thermodynamics
Digital & Optical Communications
Electronic Materials & Devices
Laser Physics & Applications
Plasma Physics & Applications
Quantum Physics & Spectroscopy
Semiconductors & Optoelectronics
Solid State Physics & Applications

CONTRIBUTIONS

Contributions to be published in this journal should be original research works, i.e., those not already published or submitted for publication elsewhere, individual papers or letters to editor.

SUBMISSION OF MANUSCRIPTS

Manuscripts should be submitted to the editor at the mailing address:

Iraqi Journal of Applied Physics
Managing Editor
P. O. Box 55259, Baghdad 12001, IRAQ
irq_appl_phys@yahoo.com

Iraqi Journal of Applied Physics
Editor-In-Chief
P. O. Box 55159, Baghdad 12001, IRAQ
editor_ijap@yahoo.com

MANUSCRIPTS

Two copies with soft copy on a 3.5" diskette should be submitted to Editor in the following configuration:

Double-spaced one-side A4 size with 2.5 cm margins of all sides
12pt Times New Roman font
Letters should not exceed 5 pages, papers no more 20 pages and reviews are up to author.
Manuscripts presented in English only are accepted.
Authors confirm affiliations, addresses and emails. Email is necessary for correspondences.
English abstract not exceed 150 words
4 keywords (at least) should be maintained on (PACS preferred)
Author(s) should express all quantities in SI units
Equations should be written in equation form (italic and symbolic)
Figures and Tables should be separated from text
Figures and diagrams can be submitted in colors for assessment and they will be returned to authors after provide printable copies
Charts should be indicated by the software used for
Only original or high-resolution scanner photos are accepted
References are written in titles, full-name authors, names of publications, years, volumes, issues and pages (from-to)

PROOFS

Authors will receive proofs of papers and are requested to return one corrected hard copy with a WORD copy on a 3.5" diskette. New materials inserted in the original text without Editor permission may cause rejection of paper.

COPYRIGHT FORM

Author(s) will be asked to transfer copyrights of the article to the Journal soon after acceptance of it. This will ensure the widest possible dissemination of information.

OFFPRINTS

Authors will receive offprints free of charge and any additional offprints can be ordered.

SUBSCRIPTION AND ORDERS

Annual fees (4 issues per year) of subscription are:

36 000 Iraqi dinars for individuals and establishments inside Iraq.
50 US$ for individuals and establishments abroad.

Fees are reduced by 25% for **I.S.A.R.E.S.T.** members. Orders of issues can be submitted by contacting the editor-in-chief or editorial secretary to maintain the address of issue delivery and payment way.

THE IRAQI JOURNAL OF APPLIED PHYSICS
EDITORIAL BOARD
P. O. Box 55259, Baghdad 12001, IRAQ
Email: editor_ijap@yahoo.com

COPYRIGHY RELEASE

Iraqi Journal of Applied Physics (IJAP)

We, the undersigned, the author/authors of the article titled

……

……

……

……

that is presented to the Iraqi Journal of Applied Physics (IJAP) for publication, declare that we have neither taken part or full text from any published work by others, nor presented or published it elsewhere in any other journal. We also declare transferring copyrights and conduct of this article to the Iraqi Journal of Applied Physics (IJAP) after accepting it for publication.

The authors will keep the following rights:

1. **Possession of the article such as patent rights.**
2. **Free of charge use of the article or part of it in any future work by the authors such as books and lecture notes without referring to the IJAP.**
3. **Republishing the article for any personal purposes of the authors after taking journal permission.**

To be signed by all authors:

Signature:…………………………………………………..date: ………………………………………..
Printed name: ………………………………………………………………………………………..
Signature:…………………………………………………..date: ………………………………………..
Printed name: ………………………………………………………………………………………..
Signature:…………………………………………………..date: ………………………………………..
Printed name: ………………………………………………………………………………………..

Correspondence address:
……
……
Telephone:………………………Fax:…………………………………..email: ………………………………….

Note: Please complete and sign this form and mail it to the below address with your manuscript

The Iraqi Journal of Applied Physics,
P. O. Box 55259, Baghdad 12001, IRAQ
Email: irq_appl_phys@yahoo.com or editor_ijap@yahoo.com, Mobile: +964-7901274190

IRAQI JOURNAL OF APPLIED PHYSICS

CONTENTS